Bachelor thesis

Preliminary design of an unmanned aerial vehicle with application to photovoltaic farm inspection

Author: Roman Esteban Hofer
Tutor: Manuel Fernando Soler Arnedo
Degree: Aerospace engineering
Date: Academic year 2014-2015

Acknowledgments

First of all I would like to thank the University Carlos III of Madrid for the education received in the past four year. I have learnt a lot and I have met a lot of incredible people. The University Carlos III also gave me the opportunity of spending an incredible year in the United States of America as part of an exchange program. I would also like too specially thank Manuel Fernando Soler Arnedo, tutor of this bachelor thesis, for giving me the idea of researching this emergent and interesting field and also for his support and understanding.

Abstract

In the past two decades there has been an exponential growth of photovoltaic power stations supported by governments all over the world. The main concern is to explore a cost-effective, reliable, and cost-saving method for determining performance and failure of photovoltaic modules. This project aims at studying the feasibility and the use of unmanned aerial systems for monitoring and detecting anomalies in photovoltaic plants. This research includes the analysis of different unmanned aerial vehicle configurations to evaluate which is the most suitable vehicle for the mission, a preliminary design of this vehicle and the investigation of thermal cameras which are efficient monitoring tools.

The methodology followed to fulfill this project started by classifying the different fields that comprise the design of a quadrotor: study of the mission, selection of the airframe configuration, payload analysis, propulsion analysis, structural analysis, and performance and dynamics. The information for each chapter was collected by using books and webpages specialized in each field. The equations presented throughout the project were solved by using Matlab and the figures were created with Excel.

Contents

List of Figures

List of Tables

Chapter 1

Introduction

As a result of climate change, dependency on oil and other fossil-fuels, the increase of importation and the raise of the cost of energy, governments are looking for alternative energy. Renewable energy is one of the most promissing solutions to the above mentioned problems: it reduces greenhouse gas emissions and contamination and it takes advantage of unlimited, localized and decentralized sources of energy like sun, wind, sea and biomass. These sources of energy avoid the volatility of the financial markets of fossil-fuels and provide employment, technological advance and economic growth. It is unquestionable that renewable energies constitute a key element for a sustainable future. Scientists have predicted that an additional of 30 TW of energy will be needed by year 2050 in order to satisfy humans demand. The photovoltaic (PV) energy is one of the most important pillars that will help to achieve this target. Photovoltaics is the method of converting solar radiation into electrical energy. It has many advantages: the energy produced is environmentally friendly; the process is noise-free; it is a locally available resource which allows avoiding transportation and decreases dependency on imported oil.

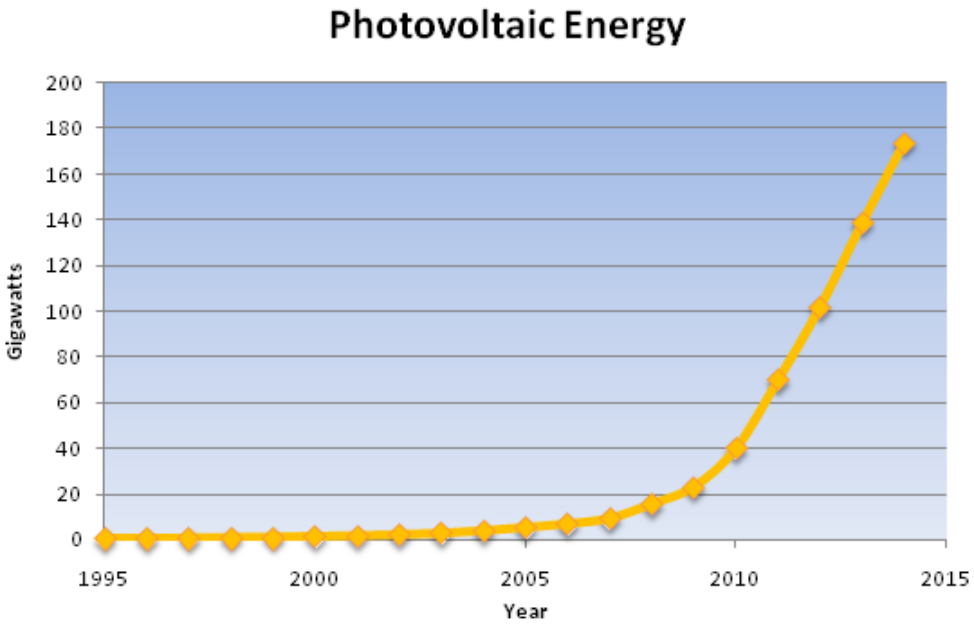

Figure 1.1: PV world capacity, 1995-2014.
Data retreived from "Global market outlook for photovoltaics 2014-2018"

The solar PV market is seeing years of extraordinary growth and it is projected that the

capacity will continue expanding, as can be appreciated in figure 1. At the moment the capacity is 174 Gigawatts which corresponds to 0.85 % of the world total electricity demand [1]. The energy is produced in PV power stations. In order to assure an efficient use of these installations, maintenance and monitoring is essential to guarantee the performance and reliability of PV systems.

1.1 The organization and functioning of PV systems

Herein we give a brief overview of the functioning of PV fields. PV fields are organized in an array of solar panels so positioned that they face the sun in the most efficient manner. A solar panel is constituted by a set of electrically connected solar modules and these modules are organized by groups of solar cells. These cells are responsible for the conversion of sun light into electricity. They are formed by semiconductors as silicon, which is currently used most commonly. When light strikes the cell, a portion of it will be absorbed within the semiconductor. The energy absorbed allows the electrons to move freely creating a current which will be drawn for external use.

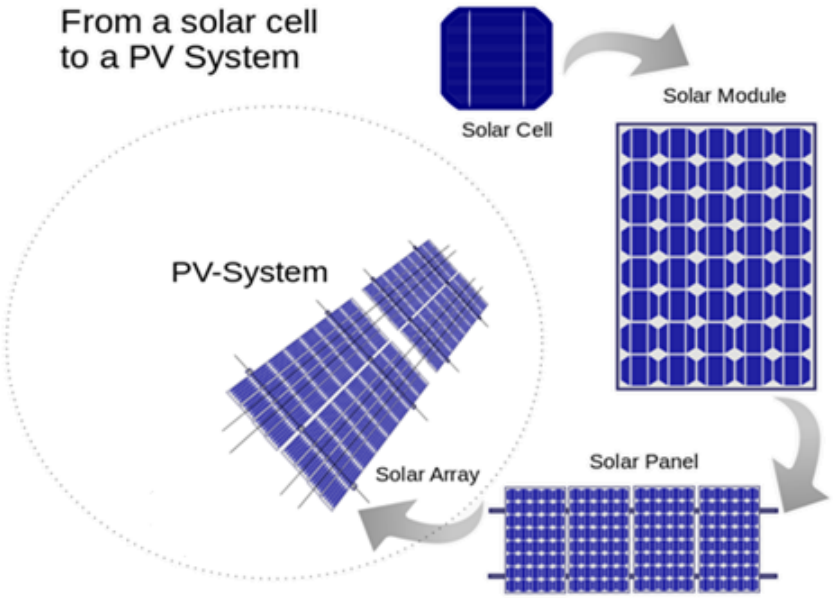

Figure 1.2: The PV system.
Source:*http* : *//en.wikipedia.org/wiki/Photovoltaic_system*

The connection between the different elements (cells, modules, panels) can be made in series or in parallel.

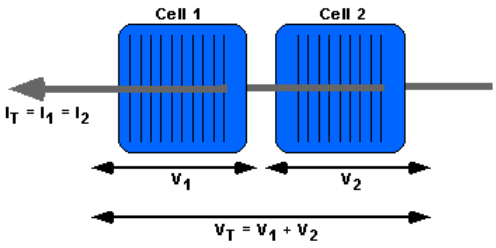

Figure 1.3: Cells connected in series.
Source:
http : //pveducation.org/pvcdrom/modules/mismatch − for − cells − connected − in − series

When connecting an element in series their individual voltage will be added and the current will remain constant. It is useful for obtaining a desired output voltage.

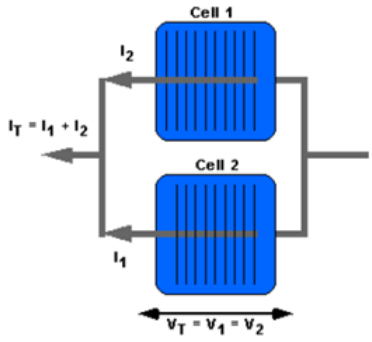

Figure 1.4: Cells connected in parallel.
Source:
http : //pveducation.org/pvcdrom/modules/mismatch − for − cells − connected − in − parallel

The voltage across an element connected in parallel remains constant while the intensity through each element will be added. It is used to boost the current output.

A PV array consists of a number of individual PV panels that have been wired together in a series and/or parallel to deliver the voltage and amperage a particular system requires. An array can be as small as a single pair of modules, or large enough to cover hectares. 12 volt module is the industry standard for battery charging. Depending on the system and its requirements the connection between all the elements will differ. Systems processing up to about 2000 watt-hours work at 12 volts. Systems processing 2000 - 7000 watt-hours will function better at 24 volt. Systems running more than 7000 watt-hours should be running at 48 volts.

1.2 Anomalies and how they affect the efficiency

When an element of a series connection has a defect/anomaly it will reduce the overall efficiency of the system or even trigger the complete failure of a module or even solar panel. The standard industrial module is constituted by 36 solar cells connected in series. The cell with an anomaly

will reduce its power output and will bring the others down to its power level. This causes an inefficient use of the installation and thus loss of profitability. Both during the production and explotation process of solar panels and solar cells a number of defects can occur. These defects are caused by mechanical forces, pressure, bad temperature control or erroneous contact at soldering points. The result is a reduction in the power output of the cell. Some of the most common defects and anomalies are listed below:

Scratches
Scratches are mostly result of improper handling at the factory or caused by unsafe packing. Manufacturers use an antireflective coating on the glass. These scratches can affect the coating impacting the transmission of light.

Broken Cells
They appear in the form of edge breakages, pinholes, V-type breakages and corner breakages. Broken Cells undermine the overall performance of the whole panel as its output is reduced to the lowest current cell. Usually broken cells are caused during soldering.

Micro cracks
Micro cracks most frequently occur during lamination of the panel or during soldering. Undetected micro cracks can result in a less than expected lifespan.

Shading effect
Another issue to take into consideration is the shading effect. PV panels are very sensitive to shading effects. Shading obstructions can be from "soft" or "hard" sources. If a tree branch, roof vent, chimney or other item is shading from a distance, the shadow is diffuse or dispersed. These soft sources significantly reduce the amount of light reaching a solar panel's cells. Hard sources are defined as those that stop light from reaching solar cells, such as a blanket, tree branch, bird dropping sitting directly on top of the glass.

1.3 The monitoring tool

Monitoring PV stations is of paramount importance for efficient power generation, long life and a high return on the investment. To ensure a good functioning of PV systems a fast, simple and reliable method to evaluate a solar panel's performance is required. The use of thermal imaging cameras for solar panel evaluation allow detecting the anomalies in a rapid manner.

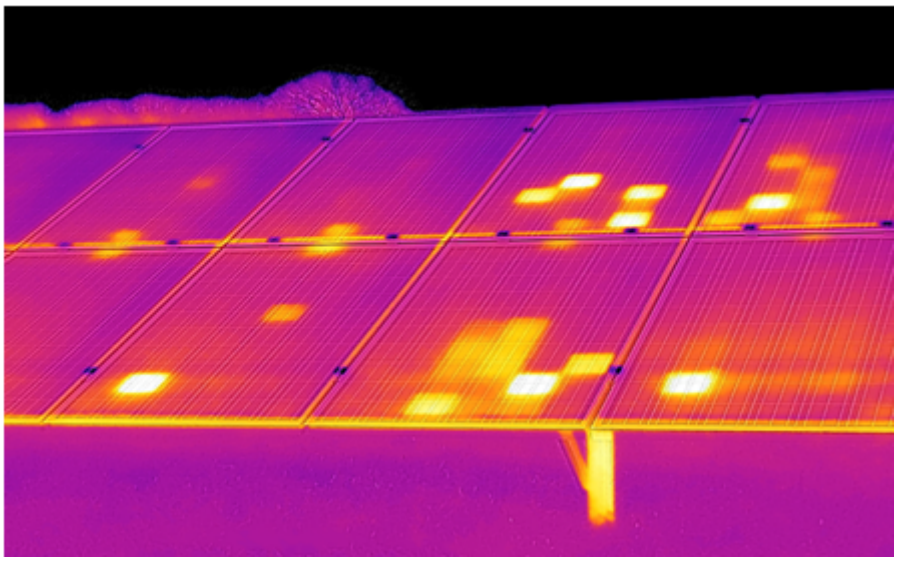

Figure 1.5: Thermal image of a set of solar panels.
Source: *http : //www.thermographicconsultancy.com/*

A defective solar cell will radiate more heat than a good functioning solar cell. With a thermal camera the hoter solar cells can be identified [2]. Depending on the shape and location, these hot spots and areas can indicate several different faults. The following table shows the typical module errors and their characteristic appearance in the thermal image.

Error type	**Example**	**Appears in the thermal iamge as**
Manufacturing defect or damage	Cracks	Cell heating, hot spot
Temporary shadowing	pollution, bird droppings	hot spots
Fauly interconnections	module not connected	module consistently hotter

Table 1.1: Typical module errors
. Source: ZAE Bayern e.V, "Überprüfung der Qualität von Photovoltaik- Modulen mittels Infrarot-Aufnahmen"

Combining a thermal camera with an unmanned aerial system (UAS) [1] allows inspecting photovoltaic fields in a faster and more effective manner.

1.4 Unmanned aerial systems

An UAS may be seen as a system comprised of a number of sub-systems that include the aircraft (referred to as unmanned aerial vehicle (UAV)). The subsystems of a UAS are listed bellow [3]:

1. As mentioned, the UAV itself which may be of many types.
2. The payload to be carried by the aircraft.
3. The electronic and control subsystem that replaces the aircew.
4. A communication subsystem which allows the interfaces between the operators and the aircraft.

[1]The terms RPAS and unmanned aircraft system (UAS) can be used interchangeably. RPAS is the term used by the international civil aviation organization (ICAO). Throughout this project the terms UAS and unmanned aerial vehicle (UAV) are used.

5. Aircraft launch and recovery subsystem
6. The operators controlling the aircraft.

1.4.1 Applications of UAS

Unammed aircraft systems are being used for a vast variety of applications. Some of them are listed bellow [3]:

1. Aerial photography: Film and video.
2. Agriculture: Crop monitoring and spraying.
3. Coastguard: Search and rescue, coastline and sea-lane monitoring.
4. Electricity companies: Powerline inspection, photovoltaic field inspections.
5. Fire services and forestry: Fire detection.
6. Meteorological services: Sampling and analysis of atmosphere for forecasting.
7. Traffic agencies: Monitoring and control of road traffic.
8. Police authorities: Search for missing persons, security and incident surveillance.
9. Military: Reconoissance, surveillance, attack.

1.4.2 Airframe configurations

There is a wide variety of airframe configurations available for UAV. Depending on the mission requirements one configuration will be more suited than the other. The different configurations can be classified into horizontal take-off and landing (HTOL) and vertical take-off and landing (VTOL). There also exist hybrid vehicles which combine the properties of both HTOL and VTOL configurations, however these will not be adressed.

1. HTOL configurations [3]

   (a) Main wing forward with control surfaces aft
   This configuration is considered as the conventional arrangement. Aerodynamic speed and attitude stability in the horizontal plane is provided by having the centre of mass forward of the wing centre of lift balanced by a down-load on the tailplane. Weathercock stability is achieved through a vertical fin and roll stability through wing dihedral.

   (b) Canard Configuration
   Canard/tandem wings use a lifting wing in front of the main wing for stability. This offers greater overall lift when compared to a monoplane, as the control surface also produces lift. With this configuration, the main wing is positioned in the downwash induced by the canard or forward wing. This can increase the induced drag from the main wing, which decreases the overall lift to drag performance. Furthermore, the canard/tandem wing configuration can suffer from a high stall speed due to the canard/forward wing stalling before the main wing.

   (c) Flying-wing
   The flying wing configuration is expected to have the best lift to drag ratio because of the minimal wetted and frontal area. The flying wing is also expected to be the lightest, as this configuration does not require structure for the tail section. Since

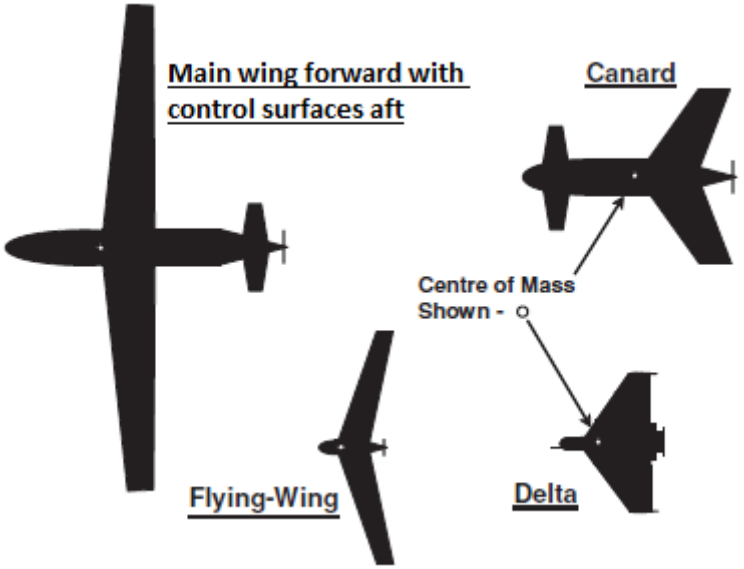

Figure 1.6: HTOL configurations
Source: Unmanned aircraft systems, UAVS design, development and deployment, 2010: John Wiley & Sons Ltd, West Sussex. p. 35

pitch and yaw stability must come from either the wing itself or surfaces attached to it, there are stability issues associated with this configuration. This reduces the moment arm of these control surfaces, reducing control authority.

(d) Delta-wing configuration

The delta-wing configuration is suitable for skid or parachute landings, without the lighter and more vulnerable tail. It has a lower gust response due to its lower aspect ratio compared to other configurations. The disadvantage is a poor lift distribution, resulting in higher induced drag intensified by its higher span loading.

2. VTOL configurations [3]

(a) Single Rotor

A single rotor configuration consits of two rotors: the main rotor and a smaller, side-thrusting tail rotor which counteracts the torque produced by the main rotor and tends to spin the aircraft. The advantages are hover and slow flight capability and vertical take-off and landing which is useful in cases where there is no runway. A disadvantage is that the aircraft is extremely asymmetric in all planes which adds to the complication of control. The tail rotor is relatively fragile and vulnerable to striking ground objects.

(b) Multi rotor

A multirotor is a rotorcraft with more than two rotors. The advantage is the simpler rotor mechanics for flight control: the vehicle changes its attitude by varying the relative speed of each rotor to produce different thrusts and torques. Another advantage is the hover and slowflight ability. The disadvantage is reduced endurance since the lift is generated aswell through the rotors guiding to a higher battery consumption.

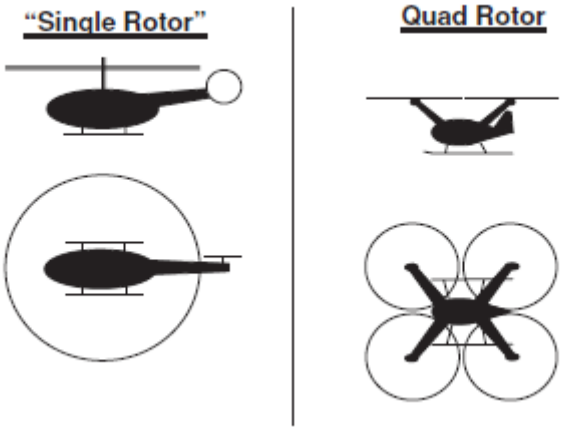

Figure 1.7: VTOL configurations
Source: Unmanned aircraft systems, UAVS design, development and deployment, 2010: John Wiley & Sons Ltd, West Sussex. p. 37

1.5 Aim of the project

The objective of this project is to provide a solution to the detection of anomalies on solar panels by combining two emerging technologies: thermal imaging cameras and unmanned aerial vehicles. The aim is to obtain the area that the UAV is capable of monitoring in one single flight to determine the viability of using UAVs for the inspection of photovoltaic power stations.

1.6 Contributions

By combining a UAV with a thermal image camera it is expected to provide a faster, simplier and cost-effective method to the detection of anomalies on solar panels. The currently used method involves an operator with a thermal image camera walking from panel to panel to detect these anomalies. The use of an UAV would greatly decrease the monitoring time and the cost.

1.7 Organization of the project

This document is structured in 8 chapters. The first chapter included the introduction explaining what a PV system and a unmanned aircraft system is. Chapter II lists the requirements to fulfill the mission and the UAV configuration which best adapts to the needs of the mission is chosen. Chapter III studies the payload requirement of the UAV. Several thermal cameras and their technical specifications are compared in order to select the most appropiate one. In Chapter IV the selection of the propoulsion system is carried out. The propulsion system is composed of the electric motor, propeller, battery and electronic speed controller (ESC). Chapter V presents different materials used for UAV frames and a structural analysis performed with Abaqus, a finite element software. Chapter VI includes a preliminary study of the 2D equations of motions of the UAV. Here the power required for hover, climb and forward flight is obtained to have an idea of the endurance of the UAV. In Chapter VII the missing components needed for the complete UAV are selected and the cost analysis is presented. Finally, in chapter VIII some conclusions are drawn.

Chapter 2

Selection of vehicle

In the previous chapter the importance of monitoring PV stations was highlighted. Combining a UAV with a thermal camera adds the advantage of inspecting large areas in short times. By defining flight segments the UAV is able to fly autonomously through a PV field recording or photographing the solar panels. Once the UAV has landed the information captured by the thermal camera can be uploaded to a computer and examined. Anomalies are detected and classified into different categories. The defects found on the panels can be monitored and if required, repaired. There are several configurations of UAV, each of them with its advantages and disadvantages. The intention of this chapter is to choose the UAV which best adjusts to the needs of the mission.

2.1 Design requirements

The first step in the design process is to summarize and understand the customer requirements for the system. The impact of each requirement on the design of the system is considered before and throughout the remainder of the design process. The customer requirements are divided into three main categories: sensor, mission requirements and weight requirements.

2.1.1 Sensor requirements

The sensor requirements dictate that the aircraft must contain a camera system capable of acquiring images in the infrared band so that anomalies on solar panels are localized.

2.1.2 Mission requirements

The mission profile can be seen in figure 4.3. First, the aircraft must take off without the use of a prepared runway. After takeoff, the aircraft will image the mission area, which consists of a photovoltaic field. After imaging the field, the aircraft will cruise back to the launch and recovery site and land without use of a prepared runway. An unskilled user must be able to successfully complete the entire mission with no low-level user control. There is not a characteristic length for photovoltaic power stations. A photovoltaic power station can be as small as 1 hectare or as big as 100 or more hectares.

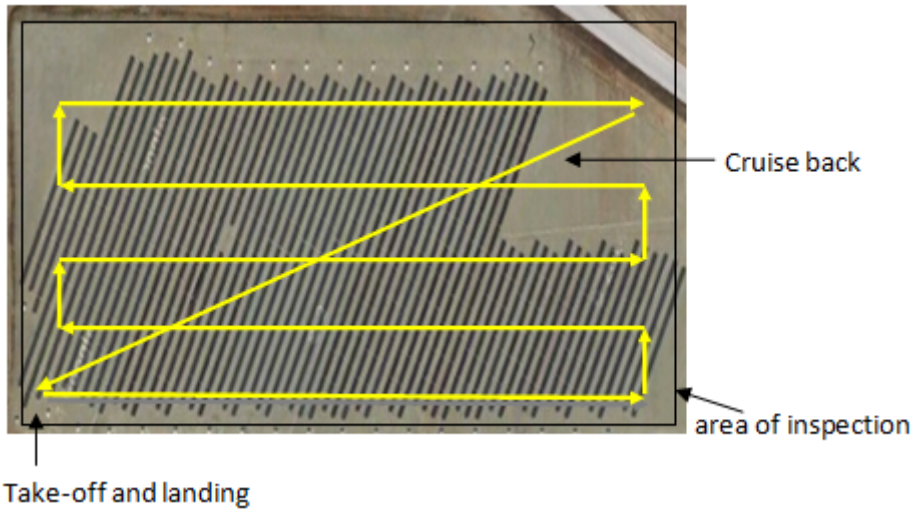

Figure 2.1: Mission summary

2.1.3 Mass requirements

In section 6 "Aeronaves civiles pilotadas por control remoto" from "boletín oficial del estado" UAVs are classified into three groups depending on their weight. Each classification has its restrictions.

1. UAV with maximum take off weight bellow 2 kg

   Beyond line of sight operations are allowed whenever the UAV remains in the range of the control station and at a maximum altitude of 120m above ground level. The position of the UAV has always to be known. The allowance to fly requires the emision of a notice to airmen (NOTAM).

2. UAV with maximum take off weight between 2kg and 25 kg

   Line of sight operations are allowed at a maximum distance of 500 m from the pilot and a maximum altitude of 120 m.

3. UAV with maximum take off weight between 25 kg and 150 kg

   Are only allowed to operate under the limitations and conditions established in their certificate of airworthiness issued by the "Agencia Estatal de Seguridad Aérea" and only in uncontrolled airspace.

Photovoltaic power stations may have dimensions larger than 500 m. In order to have the benefit of beyond line of sight operations, the weight of the UAV is required to be bellow 2 kg.

2.2 Brainstorming

A comprehensive conceptual design process was necessary to ensure a successful aircraft, as design changes are more costly later in the design process. An objective tree and a figure of merit (FOM) were used to translate the mission requirements into design requirements, as shown in figure 2.2 and table 2.1.

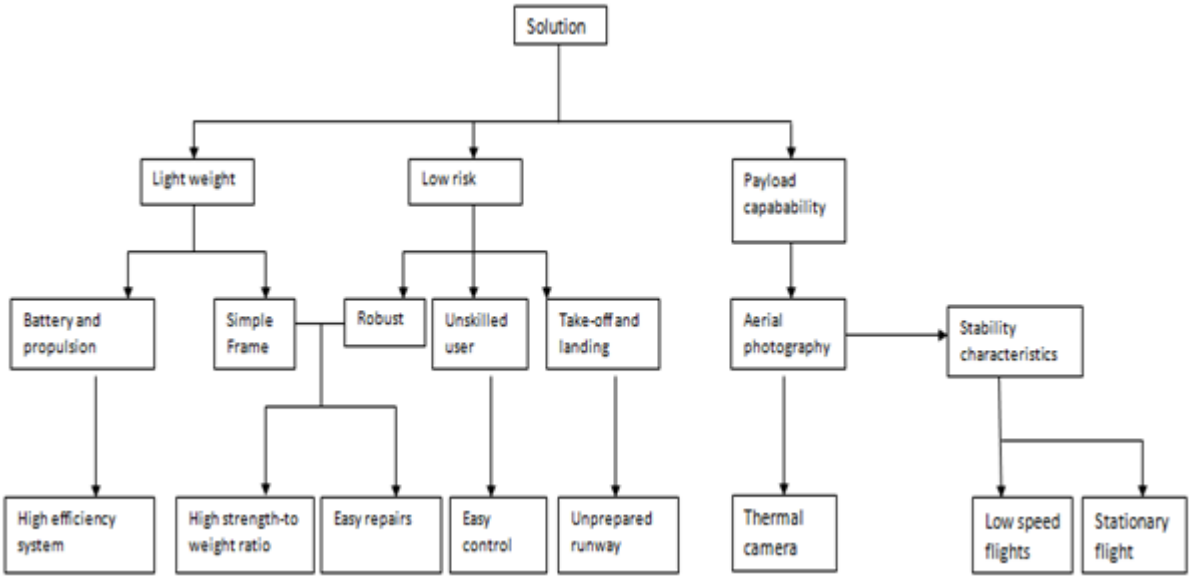

Figure 2.2: Objective tree

A FOM analysis was performed for choosing the ideal wing configuration. The different wing configurations considered were a monoplane, a flying wing and a quadrotor. Numerical values were assigned to each merit. For each merit, the highest value was assigned to the best configuration, with the other configurations rated relative to it.

Merits	**Weight**	**Monoplane**	**Quadrotor**	**Flying wing**
Takeoff and Landing	30%	4	5	3
Ease of Control	20%	3	5	2
Low/stationary speed flight	20%	4	5	2
Weight	15%	3	4	5
Range	15%	4	2	5
Final Score	100%	3.65	4.4	3.2

Table 2.1: Figure of merit

Due to its capability for vertical takeoff and landing, hovering and low speed flight the quadrotor was considered the appropiate vehicle to fulfill the mission.

2.3 The quadrotor

A quadrotor is a structure with four arms, each of which has a motor and a propeller at its end. Quadrotors are classified as rotorcraft, as opposed to fixed-wing aircraft, because their lift is generated by a set of rotors (vertically oriented propellers). Because of its unique design it allows a more stable platform, making quadcopters ideal for tasks such as surveillance and aerial photography for short range missions.

Figure 2.3: Example of a quadrotor.
Source:"*http* : *//aeroquad.com/content.php*"

2.3.1 Quadrotor control

The movement of the quadrotor is controlled by varying the relative thrusts of each rotor. In order to avoid the vehicle to spin around itself two opposite lying rotors spin on one direction, while the other two opposite lying rotors spin in the opossite direction, so that the net aerodynamic torque, and hence the angular accelaration about the yaw axis are zero. A quadcopter has four controllable degrees of freedom: Yaw, Roll, Pitch, and Altitude. Each degree of freedom can be controlled by adjusting the thrusts of each rotor. Hover or climbing are achieved by applying equal thrust to all four rotors. By applying more thrust to opposite lying propeller the vehicle adjusts its yaw. Pitch or roll are controlled by applying more thrust to one rotor and less thrust to its diametrically opposite rotor. [4]

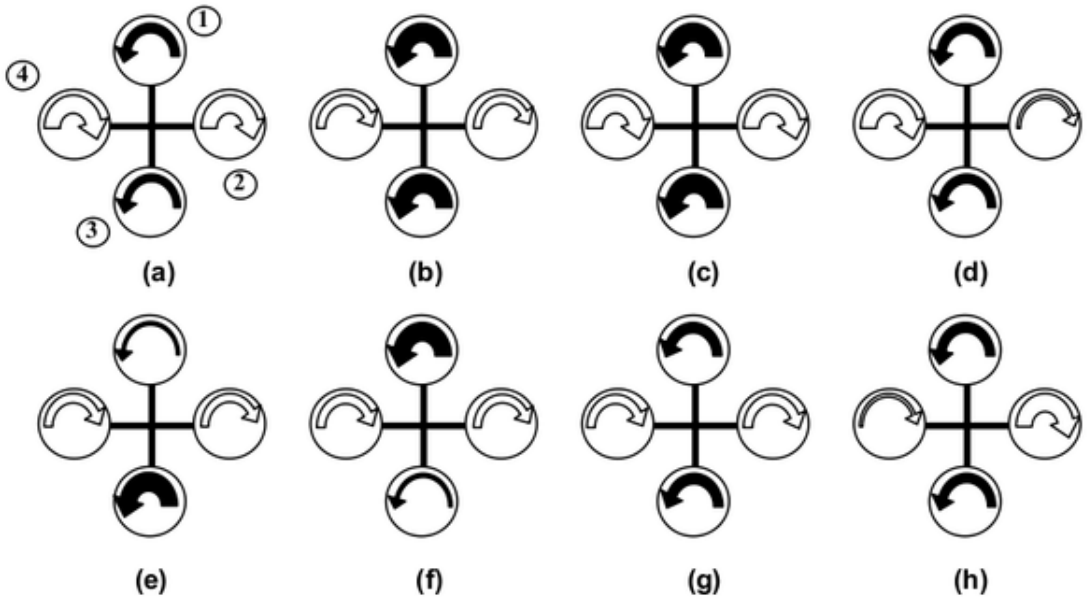

Figure 2.4: Altititude, yaw, pitch and roll control.
Source:
"$http://en.wikipedia.org/wiki/File:Quadrotor\_Motor\_Speed\_Control\_Scheme.png$"

2.3.2 Quadrotor components

The basic components that comprise a quadrotor are listed bellow [5]:

Frame
The frame is the structure that holds all the components together. It is constituted by the center plate where the electronics are mounted, four arms connected to the center plate, four motor brackets where the motors are installed and four landing skids to avoid damaging the structure. The most common materials used for the frames are aluinium, wood or carbon fiber.

Electronic speed controller (ESC)
An electronic speed controller (ESC) is an electronic circuit which varies the electric motor's speed. Since brushless motors are multi-phased, direct supply of direct current (DC) power will not turn the motors on. The ESC generates three high frequency signals with different but controllable phases continually to keep the motor turning.

Propeller
By means of the motor the propellers are spinned generating the thrust and the lift of the quadrotor.

Propulsion system
Quadrotors use brushless motors, because of their increased efficiency, longer lifetime,

reduced noise and increased reliability compared to brushed motors. Brushless motors have three coils in the inner of the motor, which are fixed to the mounting. A number of magnets are mounted to a cylinder that is attached to the rotating shaft. Coils are fixed which means wires can be connected directly and there is no need for a brush.

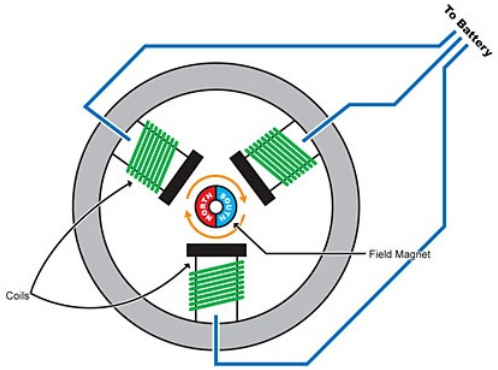

Figure 2.5: Internal view of a brushless motor.
Source:"*www.hpieurope.com/walk.php?lang = en&id = 21*"

Power system

In order to feed the motors and the other electronic onboard systems a battery is needed. There are many types of batteries, but Lipo batteries are the recommended and most used ones. They have a greater energy density making them lighter compared to other battery types.

Inertial measurement system (IMU)

An inertial measurement system (IMU) is an electronic sensor device that measures the orientation, velocity and acceleration of the quadrotor. These measurements allow the controlling electronics to calculate the changes in the motor speeds. The IMU is a combination of the 3-axis accelerometer and 3-axis gyroscope, together they represent a 6DOF IMU. Sometimes there is also an additional 3-axis magnetometer for better yaw stability (in total 9DOF).

Flight controller

The flight controller is the system that controls the quadrotor. It receives the input from the IMU and the radio control (RC) transmitter to send an output to the ESC to control the motors and adjust the flight path.

GPS module

A GPS module can be incorporated to the flight controller so that the quadrotor is able to measure its position, heading and velocity. Together with the rest of the mentioned components, the quadrotor is capable of flying autonomously.

RC transmitter

The RC transmitter is the device that the operator uses to manually control the quadrotor.

Receiver

The radio signals send by the transmitter are received by the receiver which is connected to the flight controller. The flight controller then processes the received information.

Chapter 3

Selection of payload

Selecting the thermal camera is a crucial step in the design process. It allows performing an initial weight estimate and conditions the trajectory of the UAV. Throughout the flight the UAV takes consecutive pictures or a video of the area that has to be monitored. Each photograph taken has a field of view (FOV), which defines the area that can be captured by a single image. The multiplication of the horizontal field of view (HFOV) and the vertical field of view (VFOV) is equal to the FOV [7].

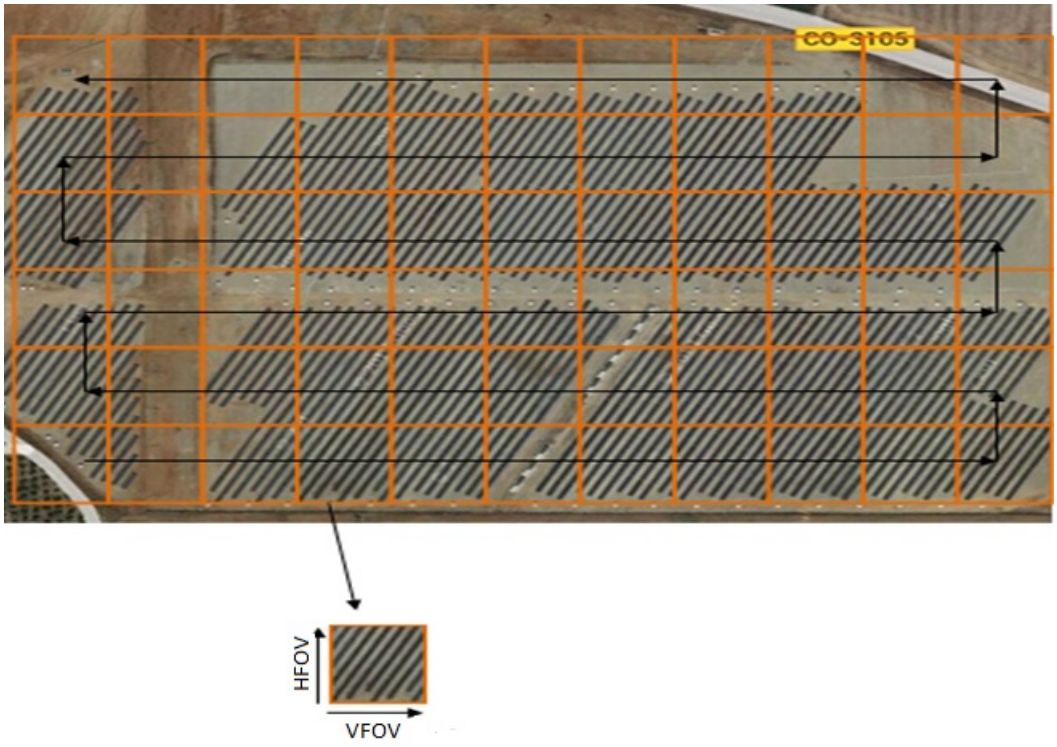

Figure 3.1: Imaging strategy to inspect PV field.

Figure 3.1 shows the possible trajectory of the UAV inspecting a PV field. The arrows represent the trajectory and the rectangles represent the FOV of each photograph taken.

3.1 Basics of thermal imaging cameras

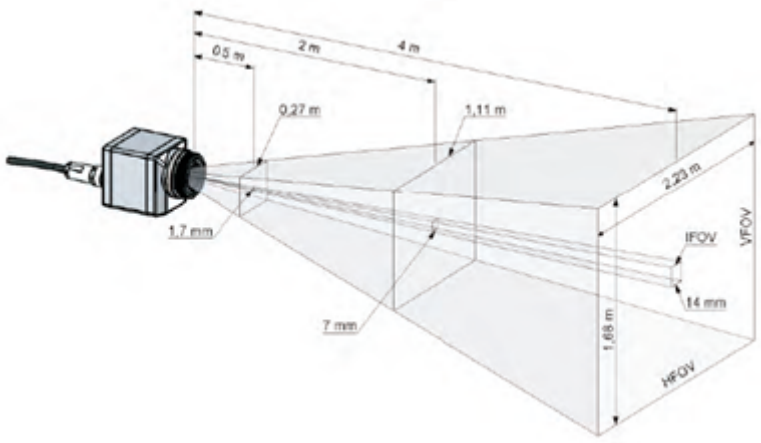

Figure 3.2: Field of view concept.
Source:"*www.optris.es*"

Figure 3.2 illustrates how the field of view increases with greater distance to target. A photograph is composed by a set of pixels. The field of view of a single pixel is called instantaneous field of view (IFOV) and defines the spatial resolution, or the size of the smallest object that can be resolved at a specific distance from the camera. IFOV increases with greater distance to target guiding to a decrease in image resolution, in other words a poorer image detail. Another important concept in thermography is the measured field of view (MFOV). It is the designation of the smallest object that can be accurately measured by a thermal camera. By general rule the MFOV is three times the IFOV. [6]

3.2 Impact of thermal camera on trajectory

The HFOV determines the distance between flight segments: choosing a distance between flight segments smaller than HFOV will lead to overlapping of photographs which causes a reduced imaged area and selecting a distance greater than HFOV will cause areas of the PV field to not be inspected.

Another parameter impacted by the thermal camera is the flight altitude. Flying at a higher altitude allows obtaining a larger field of view and therefore inspecting a wider area throughout the entire flight time of the UAV. Nevertheless the resolution of the inspected area will be worse causing a decrease in the chances of detecting an anomaly on the solar panel. The trade-off flight altitude has to be determined so that a large FOV is obtained and the anomalies on the PV panels can be detected.

3.3 The range of a thermal camera

The distance you can see a given target with a thermal imaging camera is called the “range”. The type of thermal imaging camera, the type of lens, the size of the object to detect, and the definition of what it means to “see” a target have to be considered in order to determine the range of a thermal imaging camera.

3.3.1 The Johnson's criteria

The Johnson's criteria [8] [9] can be used to define what is meant by seeing an object. John Johnson developed criteria that relate to the effective range of infrared cameras. The Johnson criteria are widely used in the commercial marketplace to characterize thermal imaging systems. According to these criteria a distinction needs to be made between degrees of seeing a target:

Detection
In order for the observer to see whether an object is present or not the critical dimension of the target needs to be subtended by 3 or more pixels. The detection concept corresponds with the MFOV and is the maximum distance to target so that the object can still be accurately measured.

Recognition
Recognizing an object implies the observer can distinct the object, for example a car or a motorcycle. The critical dimension of the object needs to be covered by at least 9.6 pixels.

Identification
The observer can see the object and its characteristics. The distinction between a man and a woman can be made. The critical dimension of the object in question is covered by 16 pixels.

3.3.2 The size of the object to see

A defective solar cell will radiate more heat than its surroundings. This warmer area will show up in the thermal image. Therefore the size of the object to detect corresponds to the size of a solar cell. Common sizes of solar cells are listed in the table bellow:

Solar cell	Dimension
4" solar cell	103mmx103mm
5" solar cell	125mmx125mm
6" solar cell	156mmx156mm

Table 3.1: Typical dimensions for solar cells.

3.4 Selection process of the thermal camera

The selection process of the thermal camera consisted in analyzing several companies specialized in thermal cameras for UAV use. The companies investigated are the following: Flir[1], Micro Epsilon[2], Optris[3] and DRS[4]. Their cameras have the characteristic of being lightweight and small sized, which makes it attractive for longer flight times and ease of mounting on the UAV. In order to choose between the wide varieties of cameras their range, field of view and weight were compared.

[1] www.flir.com
[2] www.micro-epsilon.com
[3] www.optris.com
[4] www.drs.com

3.4.1 Ranges according to Johnson's criteria

The ranges to detect, recognize or identify an object according to Johnson's criteria are given by the following formulae:

$$R_{D,R,I} = \frac{f d_{cr}}{p P_{D,R,I}}$$

Where $R_{D,R,I}$ is the range for detection, recognizion and identification, f is the focal length of the lens defined as the distance in millimeters from the optical centre of the lens to the imaging sensor, d_{cr} is the critical dimension of the object, p is the pixel pitch of the thermal camera and $P_{D,R,I}$ are the required pixels to cover the critical dimension of the object depending on detection, recognition and identification. For the sake of clarity the figures presented next, the data presented correspond only to the chosen thermal camera. Table 3.2 contains the characteristics of range, FOV and weight of the cameras analyzed.

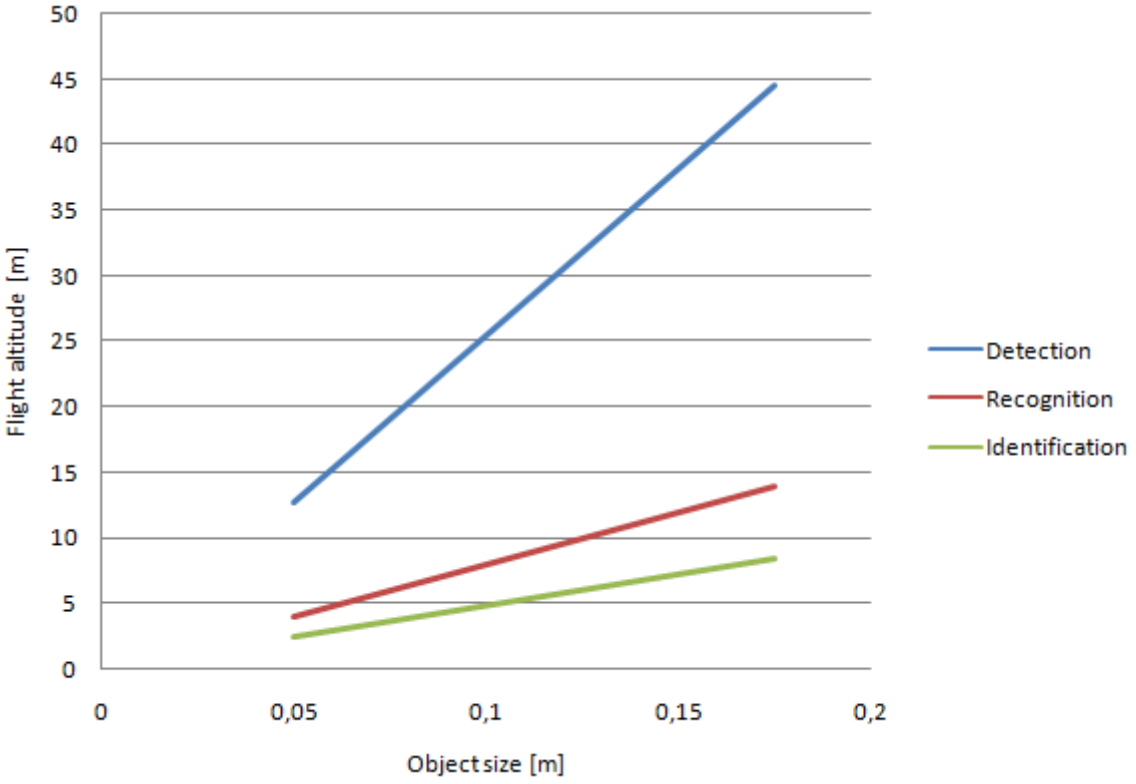

Figure 3.3: Ranges based on Johnson's criteria.

Figure 3.3 shows the different required flight altitudes for detection, recognition and identification. The x-axis represents the common sizes for solar cells. A bigger solar cell allows flying at higher altitudes. Detection range which depends upon covering the critical dimension by at least 3 pixels allows for the maximum flight altitude while still detecting the anomalies. This maximum flight altitude allows obtaining a larger field of view compared to recognition and identification range.

3.4.2 Field of view analysis

Once the dimension of the solar cell of the specific solar park to inspect is determined, the flight altitude is selected. With this flight altitude the HFOV and VFOV is obtained by the following formulae:

$$FOV_{H,V} = SensorSize_{H,V}\left(\frac{H}{f}\right),$$

where $FOV_{H,V}$ correspond to HFOV and VFOV and $SensorSize_{H,V}$ are the horizontal and vertical dimensions of the sensor of the thermal camera, respectively.

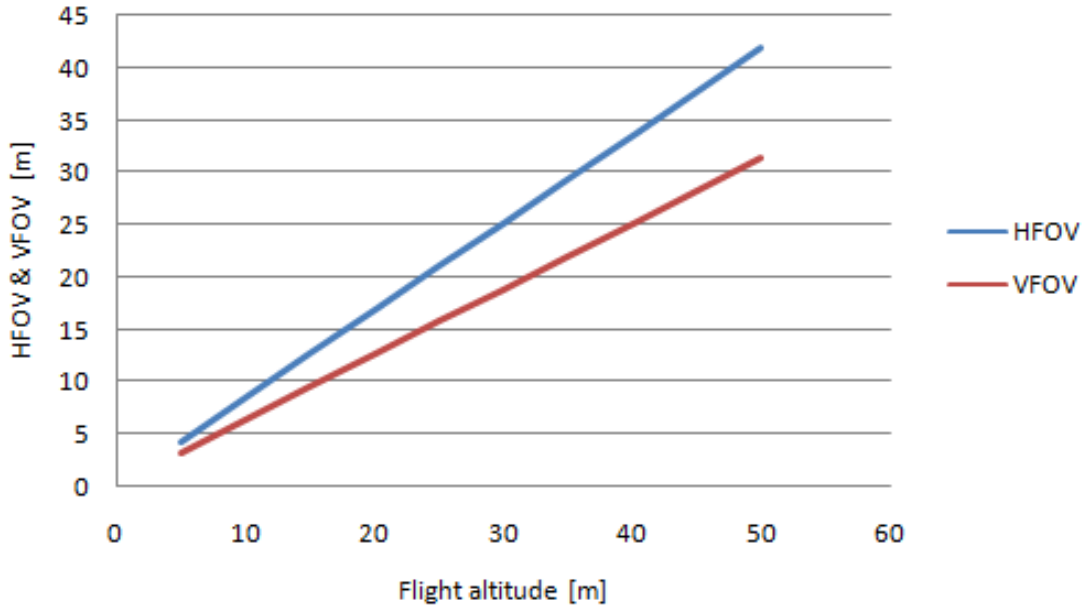

Figure 3.4: HFOV & VFOV vs. flight altitude.

The FOV of a camera is a rectangle, where the HFOV is larger. By multiplying both components the FOV is obtained. The higher the flight altitude the larger the FOV will be.

3.4.3 Resolution

With higher flight altitude and therefore wider FOV the resolution deceases so that chances of detecting a specific anomaly get reduced.

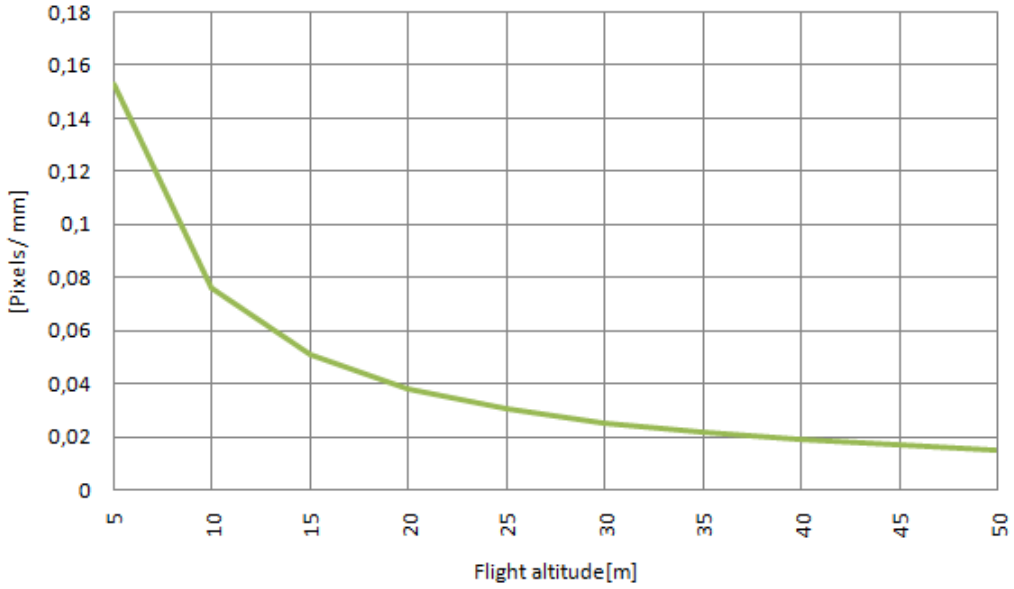

Figure 3.5: Resolution vs. flight altitude.

3.4.4 Thermal cameras comparison

The analysis presented previously was conducted for several thermal cameras. The obtained results are based on detection range of a 5' solar cell with a focal length of 13mm.

	Flir Tau 2	**Tamarisk 320**	**Tim 400**
Flight altitude [m]	32	32	22
HFOV [m]	27	13	16
VFOV [m]	20	10	12
FOV [ha]	0.054	0.013	0.0192
Resolution $[\frac{pixxel}{mm}]$	0.0239	0.0239	0.0239
Weight [g]	72	54	320
Price [$]	10072	2609	not specified

Table 3.2: Comparison of the analyzed thermal cameras.

Due to its higher FOV and reduced weight the selected thermal camera is the Flir Tau 2. A weight of 72 g has almost a negligible impact on the flying time. The wider FOV compared to the other analyzed thermal cameras allows inspecting a vaster area. The tradeoff for better performance is paid with a higher price. Flir Tau 2 costs almost 4 times the cost of the Tamarisk 320. Nevertheless a higher initial investment is considered to be more profitable since a larger FOV permits saving time and in the long term the return on the investment.

To illustrate the impact on the difference of the FOV an example is presented. Imagine a UAV with a flying time of 15 min at 15 km/h. With the Flir tau 2 an area of 10 ha can be imaged. The Tamarisk 320 would allow an area of inspection of 4.8 ha and the Tim 400 would offer an imaged area of 6 ha.

The Flir tau 2 camera specifications can be found in the annex.

Chapter 4

Propulsion system

Choosing the right motor is important for good performance in any aircraft, but it is particularly critical in a multi-rotor where both lift and thrust are produced by the motors. With the vast number of motors available, and the array of different sizes, speeds and specifications for each motor, performing a propulsion analysis is a critical task. To begin the basic selection process, we need to know how much thrust will be required to keep the UAV in the air. The design rule followed to start the selection process is that the motors should be capable of producing twice the total weight of the vehicle in maximum thrust [10]. This safety margin ensures that the motors will be capable of responding quickly to the control inputs, or arresting a rapid vertical descent, even when the battery voltage is reduced over time.

4.1 Weight estimate

The first task performed was estimating the weight of the UAV to ensure it will be possible to fulfill the weight requirement. This estimate was based on a midsized quadrotor. The average weight of the different components that form a quadrotor were invetigated. The results can be found on table 4.1

Component	**Weight [g]**
Frame	400
4xMotor	280
4xPropeller	52
4xESC	100
Flight controller	50
Thermal Camera	72
Total (without battery)	954

Table 4.1: Weight estimate.

Note that the weight estimate does not include the weight of the battery. Since the weight requirement dictates that the maximum weight of the UAV may not exceed 2 kg a battery of 1 kg can be accomodated.

4.2 Selection of the power system [11]

4.2.1 Introductory concepts of brushless motors

Figure 4.1: Typical motor used for multirotors.
Source:
"*www.hobbyking.com/hobbyking/store/__40073__NTM_Prop_Drive_Series_28_30_1200kv_400w.html*"

From the design rule each motor will have to generate a maximum thrust of 1 kg, so that when the motors are operating at 50% of maximum thrust the UAV will be hovering. The two key performance parameters when selecting a brushless DC motor are the motor constants K_v and K_t. K_v is defined as the motor voltage constant and is expressed as

$$K_v = \frac{RPM}{V},$$

where V is the voltage across the motor and RPM are the revolutions per minute. For a given battery with a specific voltage the voltage constant relates the maximum RPM at which the motor will be able to operate. This means motors with a high K_v will be able to operate at a higher RPM rate than a low K_v motor. There is a voltage drop due to the armature resitance of the motor. This voltage drop is given by $V = V_{bat} - IR_m$ where V_{bat} is the voltage from the battery, R_m the armature resitance and I the current reaching the motor. This current suffers a loss due to the no load current of the motor defined as I_0. The current I then becomes $I = I_{bat} - I_0$ being I_{bat} the current provided by the battery. The expression for K_v used above then becomes:

$$K_v = \frac{RPM}{V_{bat} - (I_{bat} - I_0)R_m},$$

which means the maximum rpm at which the motor is able to operate gets reduced with increased current input. K_t is defined as the torque constant and specifies the motors ability to produce torque for each current input. It is expressed as:

$$K_t = \frac{\tau}{I},$$

where τ is the torque. Considering the current losses due to the no load current of the motor equation becomes

$$K_t = \frac{\tau}{I_{bat} - I_0}.$$

All the constants listed are specified by the manufacturer. The torque constant and the voltage constant are related through:

$$K_t K_v = 1352.$$

K_t and K_v are inversely proportional. The product of Kt and Kv is a constant for every motor. The higher the K_v of the motor, the smaller the proppeler will need to be. Smaller propellers allow for greater speeds, but reduced efficiency. A larger propeller setup with correspondingly-low K_v motors is more efficient and will more easily mantain the stability of the UAV. For applicatios of aerial photography large propellers and low operating rpm work best. Typical values for K_v in applications of aerial photography are in the range of 700-900 [RPM/Volt]. The power that the motor can generate is given by $P = IV$. Considering the losses mentioned the power equation becomes:

$$P_{shaft} = (V_{bat} - I_{bat}R_m)(I_{bat} - I_0).$$

Note that the power increases with higher current input but the rpm limit will be lower due to the losses.

4.2.2 Introductory concepts of propellers

A motor by itself is not able to specify the amount of thrust that it will generate. For that the combination of propeller, battery and motor has to be included. For the range of K_v specified in the previous subsection, propellers with a diameter of around 10 inches are used. Propellers used for electric powered aircraft have usually two blades and are classified by lenght and pitch.

Figure 4.2: APC propeller 10x4.7SF.
Source:
"$http://www3.towerhobbies.com/cgi-bin/wti0001p?\&I=LX1684$"

For example a 10x4.7 propeller like the one shown in figure 4.2 has a diameter of 10 inches and a pitch of 4.7 inches. The pitch can be defined as the travel distance of one single propeller rotation.

Figure 4.3: Comparing propellers with different pitch.
Source:
"$www.blog.oscarliang.net/how-to-choose-motor-and-propeller-for-quadcopter$"

A propeller with low pitch numbers can generate more torque and improve stability. A higher pitch propeller can cause instabilities when hovering. Typically, multi-rotors use propellers with pitches in the range of 3 to 5 inches.

4.2.3 Introductory concepts of batteries

Lithium-ion polymer (LiPo) batteries are the most common power source for multi-rotors. They are lightweight, compact and offer high discharge rates. When selecting the battery there are a few specifications to consider. The first one is the voltage. Each cell of a LiPo battery has a voltage nominal value of 3.7V (Volts). Each additional cell wired in cell adds 3.7V to the nominal voltage of a battery. Cell counts are denoted by the number of cells followed by "S". For example a 3S Lipo battery like the one presented in figure 4.4 has a nominal voltage of 11.1V.

Figure 4.4: 3S LiPo battery.
Source:"$http://www.rcgroups.com/forums/showthread.php?t = 1441186$"

Depending on the chosen configuration of LiPo battery the brushless DC motor will able able to operate at a certain maximum rpm. A higher voltage will allow the motor and propeller combination to produce a higher maximum thrust at a cost of full throttle flight time as the current draw will increase. Another specification of batteries to consider is the capacity measured in milliamp-hours (mAh). It defines the limit of how much energy it can store. A 1000 mAh battery will be able to produce continously 1000 mA for one hour. A battery with higher capacity allows increased flight time. This is true until a certain limit, since a higher capacity battery will have a higher weight and the motors will not be able to produce the necessary power to lift this extra weight. Adding cells in parallel will increase capacity. Cells connected in parallel are denoted by the number cells followed by a "P". C-Rating is another factor to take into account. It indicates the maximum rate at which a battery can be discharged. A 70 C battery like the one from figure 4.4 will have a maximum discharge rate of 70 times its capacity which is 2200 mAh. This gives a maximum discharge rate of 15.4 amperes. This is an important specification to consider when selecting a battery since a motor might require a certain amount of amperage to spin the propeller at a specific rpm. If the required amperage exceeds the C-rate of the battery the motor will not be able spin the propeller at the desired rpm and even get damaged. The power that a battery is able to provide is given by $P = I_{bat}V_{bat}$. The internal resistance of the battery causes a voltage drop wich increases with higher current draws. This voltage drop is given by $V_{bat} = V_{nom} - I_{bat}R_{bat}$ where V_{nom} is the nominal voltage of the battery and R_{bat} is the internal resitance expressed in Ohms. The actual power provided by the battery is given by:

$$P_{bat} = I_{bat}(V_{nom} - I_{bat}R_{bat}).$$

4.2.4 Comparing various motors

In order to detect the combination of battery, motor and propeller which will generate the desired maximum thrust a software called Drive Calculator[1] is used. Drive Calculator is a tool that can be used for DC motor analysis and as an aid in the selection of the complete power system for electrically powered model aircraft. By selecting a power supply and a propeller Drive Calculator finds matching motors and lists them by the maximum static thrust that the combination can provide. For the input of power source a 3S LiPo battery is introduced. The 3S or 4S LiPo configurations are typically used. The input for the propeller is a 10x5 APC propeller. The next step was selecting a list of motors which generate 1 kg maximum thrust. These motors and their constants can be found in table 4.2.

	$K_v[\frac{RPM}{V}]$	K_t	I_0 [A]	R_m [Ω]	W [g]
Scorpion SII-3020-780	780	1.73	1.21	0.03	166
Turnigy AX-2810Q-750	750	1.80	0.82	0.095	70
E-flite Park 400-740	740	1.82	0.55	0.26	56
Hacker A30-14L-V3	800	1.69	1.6	0.036	143

Table 4.2: Analyzed motors and their constants.

To select one of the motors their efficiency and weight were compared. The efficiency of a motor is computed with the ratio of output power from the motor to input power from the battery:

$$\eta = \frac{P_{shaft}}{P_{bat}} = \frac{(V_{nom} - I_{bat}(R_{bat} + R_m))(I_{bat} - I_0)}{I_{bat}(V_{nom} - I_{bat}R_{bat})}.$$

The results for the efficiencies of the analyzed motors are shown in figure 4.5.

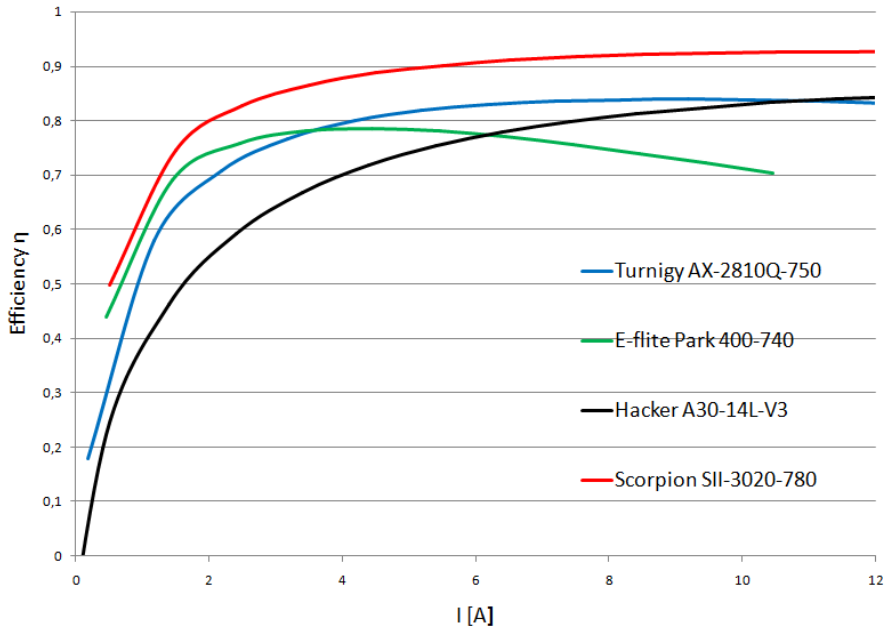

Figure 4.5: Efficiency curve for the motors presented in table 4.2.

[1] www.drivecalc.de

The other parameter considered to select the motor was the weight.

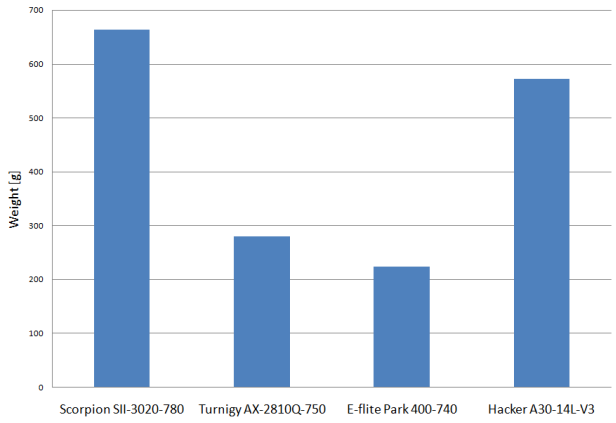

Figure 4.6: Weight of the complete set of four motors.

Figure 4.6 considers the weight of the four motors that will complete the quadrotor. By a first look at the efficiency curve one would consider choosing the Scorpion SII-3020-780 but the weight of the four motors conform a 33.2% of the maximum weight of the quadrotor reducing weight for adding a more powerful battery. Turnigy AX-2810Q-750 and E-flite Park 400-740 occupy a 14% and a 11.2% respectively of the maximum weight. This is an acceptable fraction of the total weight for adding a higher capacity battery and achieve higher flight times.

E-flite Park 400-74 presents a higher efficiency for an input current in the range of 0 to 4 A, while Turnigy AX-2810Q-750 offers a higher efficiency for values of current above 4 A. To select between these motors the current draw at hover is compared.

In order to obtain the current draw at hover the power necessary for hover has to be known. APC has computed the performance of their propellers. The thrust and the power consumed for a range of rpm and speeds can be found in their webpage[2]. In Figure 4.7 the thrust vs. power consumption at static conditions can be seen. At hover each motor lifts one fourth of the total weight. This weight is included in the figure to determine the necessary thrust to hover and hence the power consumption.

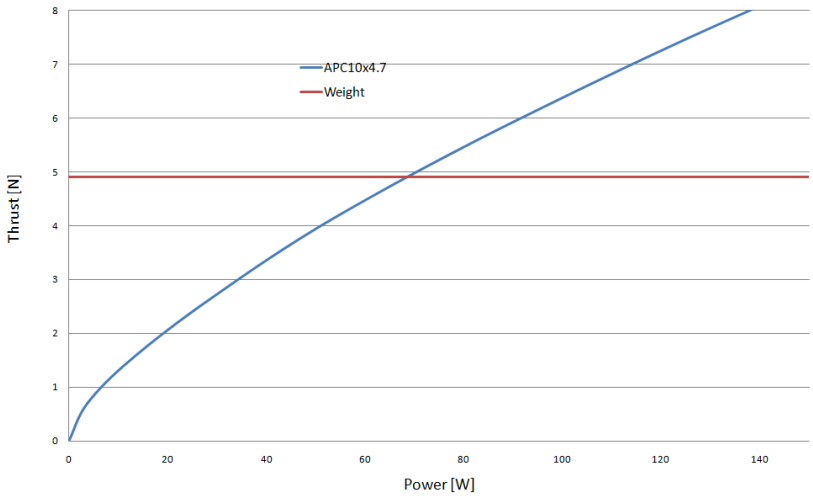

Figure 4.7: Thrust vs. power consumption.

[2]www.apcprop.com

The intersection of both curves determines that the power consumed at hover is equal to 69 Watts. To determine the current draw, the power generated by the motor per current input is computed. Using the equation of P_{shaft} leads to figure 4.8.

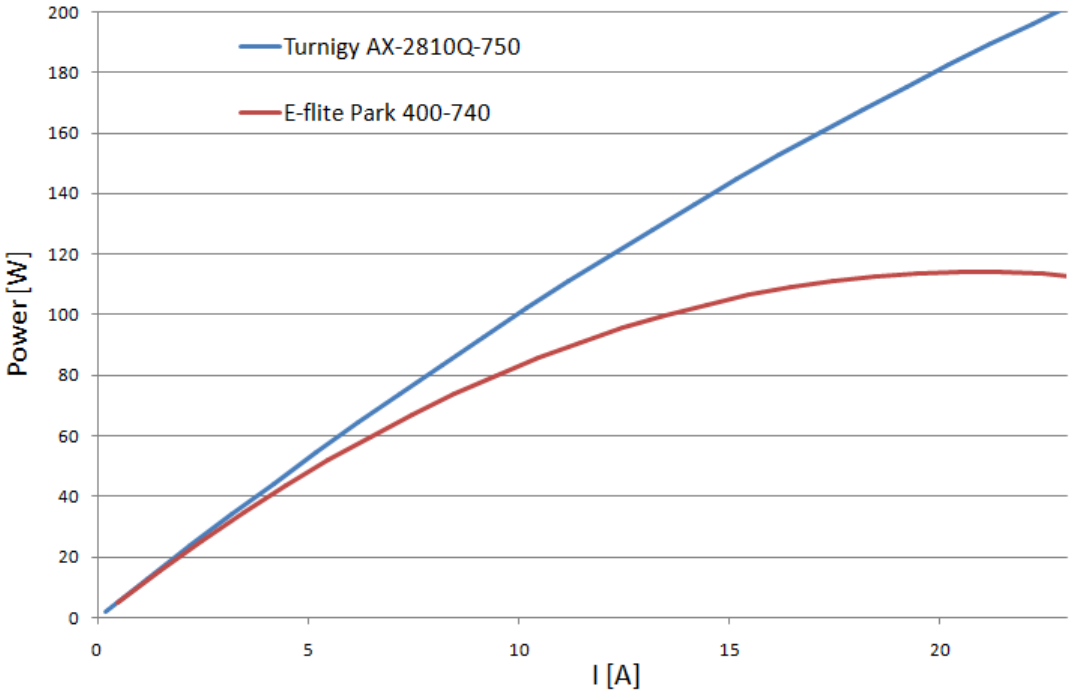

Figure 4.8: Power per current input generated for both motors.

At hover Turnigy AX-2810Q-750 requires a current input of 6.6A while E-flite Park 400-740 consumes 7.8A. The efficiency for these current inputs for both motors can be checked in figure 4.5. Turnigy AX-2810Q-750 operates an efficiency of 84% and E-flite Park 400-740 works at an efficiency of 75%. Therefore the selected motor is the Turnigy AX-2810Q-750 since it draws less current at hover conditions allowing larger flight times and operates more efficienly.

4.3 Selection of propeller

A number of propellers is compared to ensure that the motors at 50% of their maximum thrust are able to hover the vehicle. The propellers analyzed includes the suggested propeller (10x4.7 APC), plus the 11x4.7 APC and the 12x6 APC propellers. To determine the maximum thrust for each propeller, the power vs. rpm curve is used. Figure 4.9 includes the power for the maximum rpm at which the motor will be able to operate and the power consumed by the propeller for each rpm.

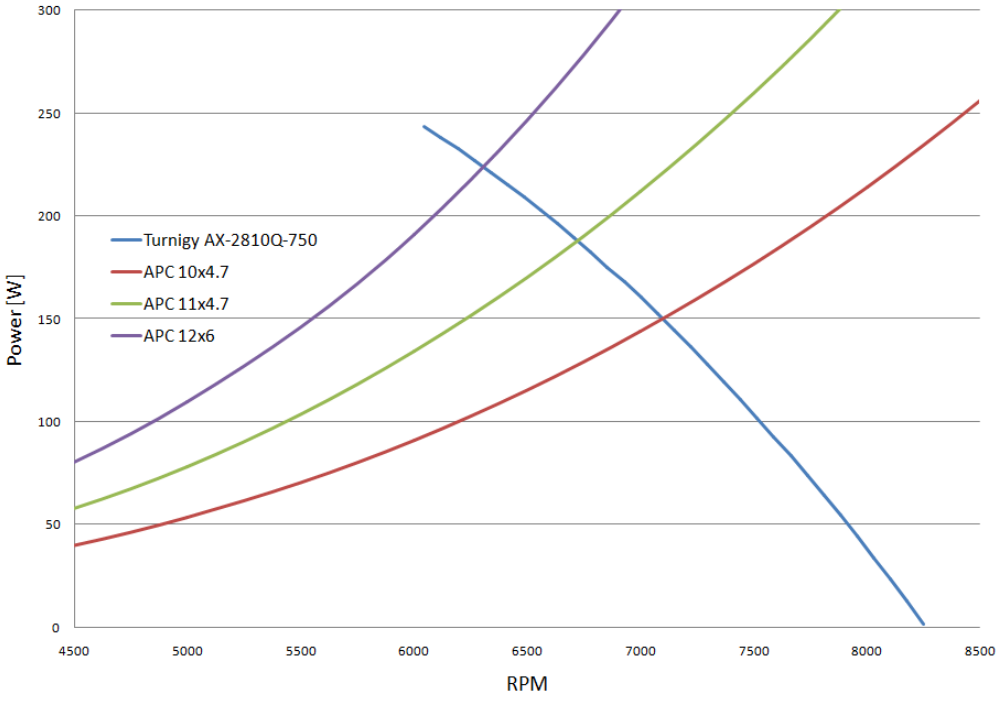

Figure 4.9: Power.

The maximum power at which each combination of motor and propeller will be able to operate is given by the intersection of the power curves. Figure 4.10 relates the power to thrust of each propeller. With the maximum power, the maximum thrust that the propeller can provide is obtained.

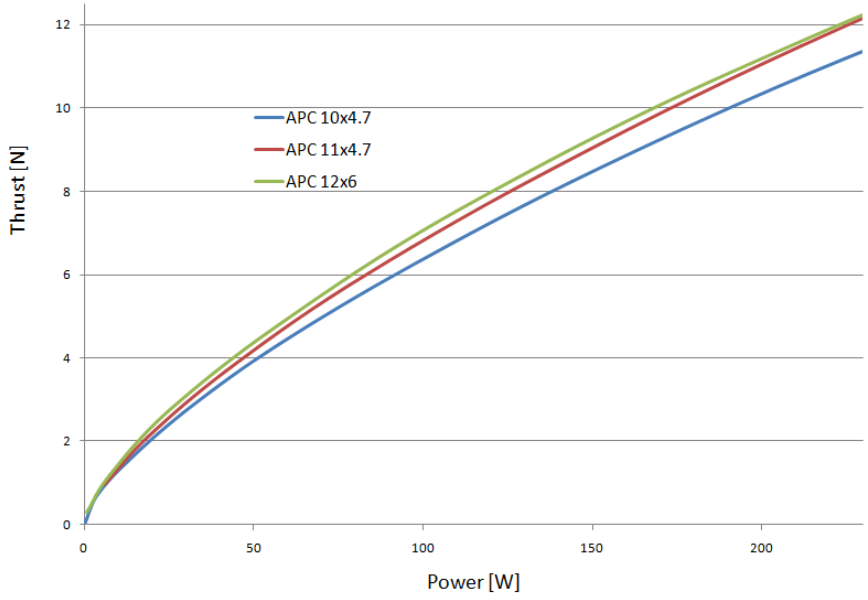

Figure 4.10: Thrust generated by propeller per power input.

The results are summarized in table 4.3.

	P_{max} [W]	T_{max} [N]	RPM_{limit}	% of T_{max} for hover
APC 10x4.7	150	8.2	7100	60%
APC 11x4.7	188	10.8	6722	45.3%
APC 12x6	223	12	6308	40.8%

Table 4.3: Analyzed propellers.

APC 11x4.7 is the appropriate propeller for the selected motor, power source and vehicle weight. For hover this combination of motor and propeller will be operating at 45.3% of maximum thrust, which is slightly bellow the design rule followed to select the motor, battery and propeller combination.

4.4 Selection of battery

The weight estimate performed in section 4.1 allows to install a battery of 1 kg without entering in conflict with the mass requirement. Table 4.4 shows a list of analyzed batteries with their corresponding characteristics.

	Voltage [V]	Capacity [mAh]	C-rating	Weight
Zippy Flightmax	11.1	3000	20C	239
Turnigy NanoTech 4500	11.1	4500	25C	361
Turnigy NanoTech 6000	11.1	6000	25C	481
Zippy Traxxas	11.1	8400	30C	614

Table 4.4: Analyzed batteries.

The trend of increased weight for increased capacity can be observed. Since there is an allowance of 1 kg of battery, the Turnigy NanoTech 6000 battery is selected. Two of these batteries connected in parallel will lead to a total battery weight of 962 gramms so that the total weight of the UAV is bellow 2 kg. By adding the batteries in parallel the capacity is doubled providing a total of 12000 mAh allowing longer flight times. Nevertheless the maximum discharge rate of the battery has to be verified before being sure that this configuration is valid. When the motor is operating at maximum power, it has to be sure that the battery is able to discharge at the required current. From table 4.3 the maximum power at which the motor is able to operate is read. Then, from figure 4.8 the current required is found. The current required for maximum power is 21 A for one motor. This means that the four motors operating at maximum power will draw 84A. Since the two batteries are connected in parallel 42A will flow from each battery. To determine if the battery will able to discharge at this rate the C-rating is multiplied by the capacity leading to maximum current discharge rate of 150A. Thus, the selected battery is valid.

4.5 Selection of the electronic speed controller

The electronic speed controller (ESC) is an electronic circuit whose purpose is varying the electric motors speed. To select an ESC the maximum current rating and the voltage rating have to be considered. The current drawn by the motor at full throttle has to be lower than the maximum current rating of the ESC, otherwise the electronic circuit will get damaged. The voltage provided by the battery has to be within the voltage limit of the ESC. With

the combination of battery, motor and propeller the current drawn at maximum throttle is 21 amperes and the voltage provided by the battery is 11.1 V, which means an ESC with a maximum current rating of 25 A and being able to handle a 3S battery will be suitable for the chosen combination.

Considering the specifications, the Q Brain 4 x 25A Brushless Quadcopter ESC is selected. It has the advantage that it incorporates four ESC into a single unit keeping the wiring very tidy and allows mounting this unit in the middle of the frame instead of having to mount an ESC on each arm. In figure 4.11 the selected ESC can be seen.

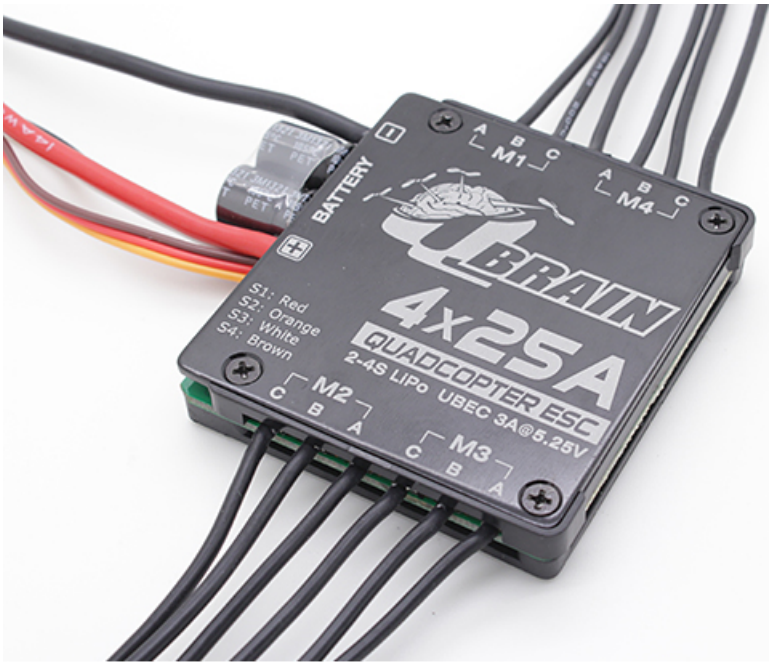

Figure 4.11: Q Brain ESC.
Source:"*www.hobbyking.com*"

Chapter 5

Structural analysis

A structural analysis is necessary to ensure that the structure of the quadrotor will be able to withstand the loads encountered in flight. The structure of a quadrotor consists of a center plate with four arms attached to it. Abaqus[1], a finite element software, is used to perform the structural analysis.

Figure 5.1: Quadrotor frame.
Source:
"*www.hobbyking.com/hobbyking/store/__24151__Hobbyking_X550_Glass_Fiber_Quadcopter_Frame_550mm.html*"

5.1 The structural model

To perform the structural analysis the arms are modeled as cantilever beams, which are beams with one end encastred and the other one free. The loads encountered on flight are the thrust and the torque generated by the propulsion system (see figure 5.2). These forces are modeled as a point load and a torque at the free end of the cantilever beam. The maximum load that the cantilever beam experiences is when the motor is operating at maximum power. This value is obtained from the analysis conducted in chapter 4. In table 4.3 one can see that the maximum

[1] www.3ds.com/products-services/simulia/products/abaqus/

thrust is 10.8 N at 6722 rpm. From the APC database the torque of the selected propeller per rpm input is obtained (see figure 5.3). At 6722 rpm the torque produced by the propeller is 0.25 Nm which is negligible compared to the thrust produced. Nevertheless it will be included in the analysis to see the complete behaviour of the structure.

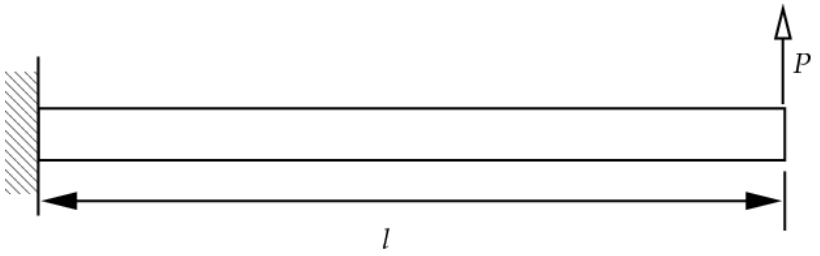

Figure 5.2: Quadrotor arm modeled as a cantilever beam with point load at free end.

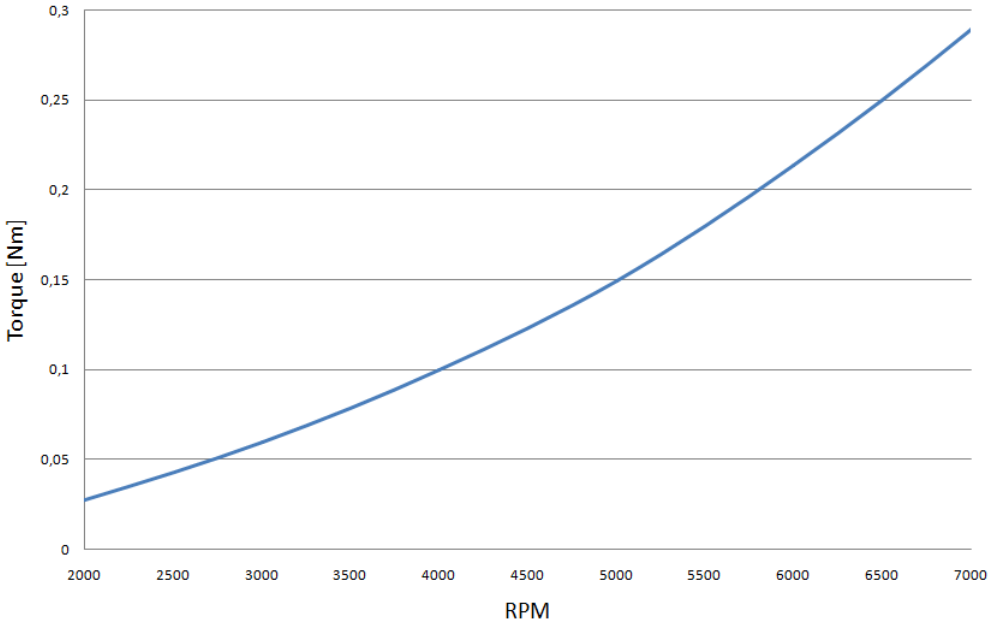

Figure 5.3: Torque produced by the propeller per rpm input.

5.2 The dimensions

An important factor to consider is the dimension of the frame. The center plate should have the correct size so that all the electronics can be mounted and the arms should be larger than the propeller radius so that there is no interference of the outcoming air of the propeller and the center plate. A larger arm also increases stability since the force produced by the motors generates a higher torque, so that the structure will react and stabilize faster to rpm changes. However a larger arm adds weight to the structure decreasing flight time. In order to determine the optimum arm distance, the equations of motion of the quadrotor have to be iterated for several arm sizes to observe how the stability and mass is affected. Nevertheless this analysis will not be considered. For a preliminary analysis a number of already constructed frames are

analyzed. Hobbyking[2], an online shop specialized in electric powered UAVs, sells a wide variety of frames. The frames analyzed were the ones that were suggested to be use with propellers of the size of 11". These frames had the characteristic of having a motor to motor distance in the range of 600 to 700 mm. With this range and considering that the largest component of the electronics is the battery a preliminary design of the frame is suggested.

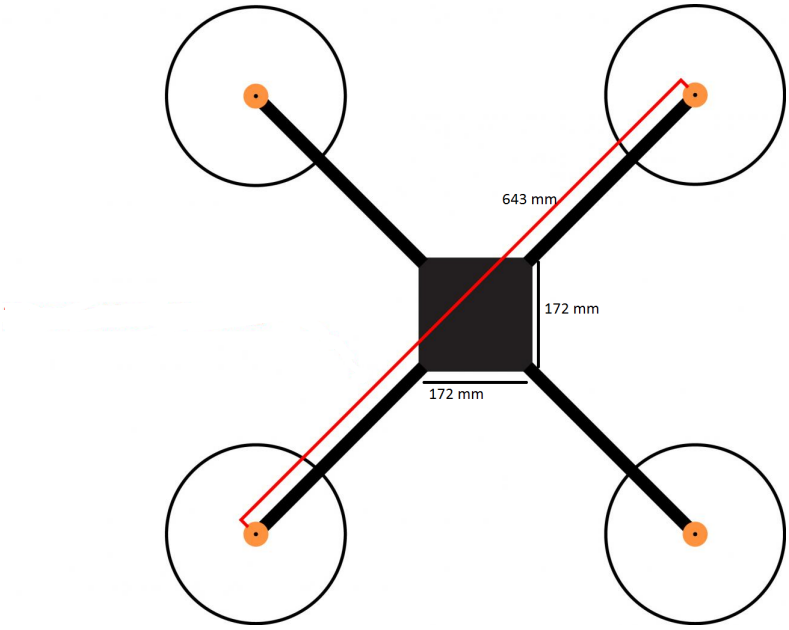

Figure 5.4: Preliminary frame.

5.3 Aluminium hollow square section beam

A common material used for the frame of the quadrotor is aluminium due to its high strenght to weight ratio. The structure presented in figure 5.4 is an example of a frame made out of aluminium. The arms of this frame present a hollow square section, which allows that the wiring to the motor goes through the inside of the arm. This is a benefit since the wiring is not exposed and is protected. This type of aluminium bar is easy to obtain from a wide variety of manufacturers. Numerous webpages of these manufacturers [3] [4] [5] were visited to found out what aluminium alloy is used by them and the sizes of the section of the beams that they offer. This will guarantee that during the construction process of the quadrotor the different pieces will be available in the market. In order to save weight the smallest size of a hollow square section beam was selected.With these dimensions and the properties of aluminium 6063-T5 (see table 5.1) an Abaqus model was created (see figure 5.6).The next step was modeling the forces acting on the arm to determine if the selected beam withstands the load and mantains its shape without detrimental deformation. To determine material failure the von Mises stress criterion [12] is used. In this case, a material is said to start yielding when the von Mises stress reaches a critical value known as the yield strength, σ_y. In table 5.1 the yield strength of aluminium can be seen. The loads were introduced separately to observe how the structure responds to each force input. Afterwards, the real case where the loads act together was analyzed.

[2] www.hobbyking.com
[3] *www.ullrich.com.au/square_tube2.php*
[4] *www.raaltd.com/aluminium − squarehollows.html*
[5] *www.onesteelmetalcentre.com/products/aluminium*

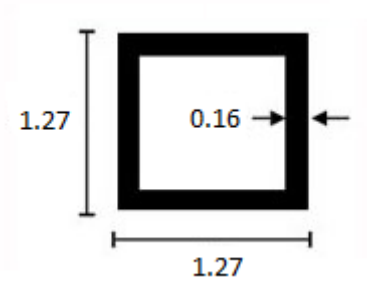

Figure 5.5: Dimension of the section in cm.

Properties	**Aluminium 6063-T5**
Young Modulus E [GPA]	68.9
Poisson's ratio ν	0.33
Yield strength σ_y [Mpa]	145
Density ρ $[kg/m^3]$	2700

Table 5.1: Mechanical properties of Aluminium 6063-T5.

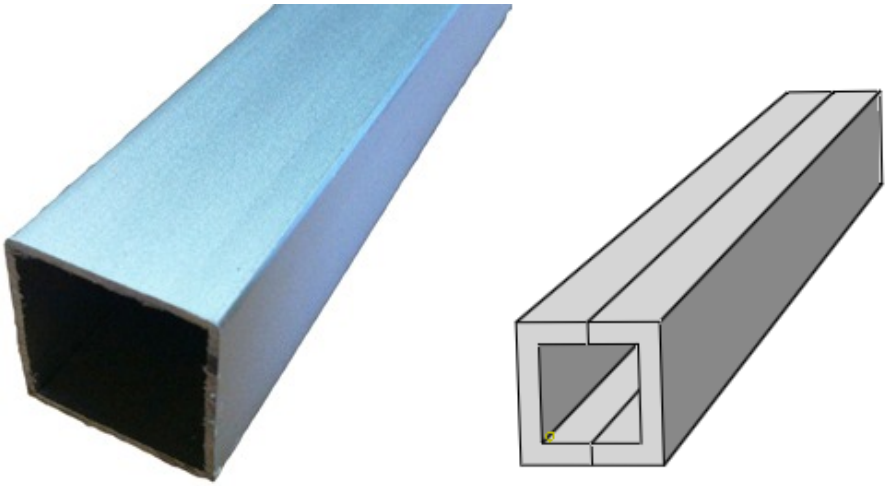

Figure 5.6: Left: Actual aluminium bar from manufacturer. Right: Abaqus model.

5.3.1 Stress and deflection due to torque of propeller

The first case studied corresponds to the load case due to the torque produced by the propeller. Figure 5.7 and figure 5.8 shows the deflection and the stress of the arm exposed to a torque produced by the propeller. The maximum displacement can be found on the free end of the arm where the motor and propeller are installed. Abaqus shows how the arm would deflect in an exagerated manner. In reality this deflection is not observable since the maximum deflection has a value of $5.4E^{-}5m$. Thanks to the torque produced by the propellers, the UAV is able to yaw. The torque produces a force that rotates the arm to the right. When all the propellers spin at the same rate the net torque is cancelled out but when two opposite lying propellers spin at a higher rate than the other two opposite lying propellers the structure rotates in the yaw

plane. The area in red of the beam depicted in figure 5.7 shows where the stress is the highest. It can be observed that the stress accumulates in the web of the beam, being the left web in tension and the right web in compression. The maximum von Mises stress of the structure is 0.9 Mpa which is well bellow the yield strenght of Aluminium (see table 5.1).

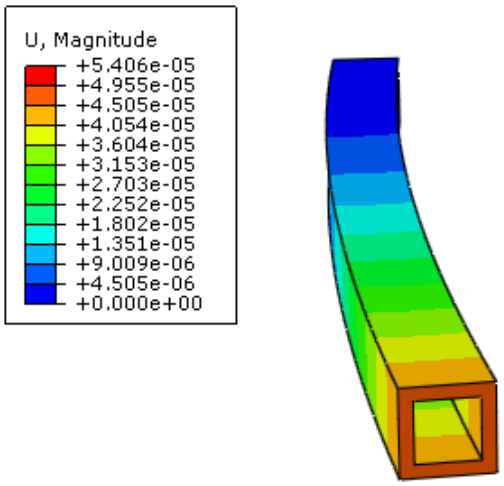

Figure 5.7: Deflection due to the torque of propeller.

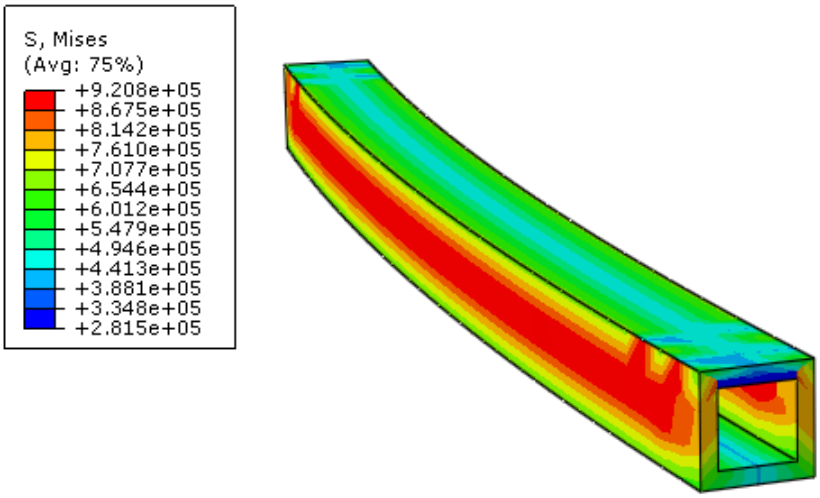

Figure 5.8: Stress due to the torque of propeller.

5.3.2 Stress and deflection due to thrust of propeller

Figure 5.9 and Figure 5.10 depicts the deflection and the stress caused by the thrust of the propeller, which produces an upward force pushing the structure up. By generating a higher thrust at an opposite lying propeller, the quadrotor is able to produce pitch and roll moments. In this scenario the flanges are the responsible of withstanding the stresses. The maximum von Mises stresses are found at the root of the beam with a value of 7.8 Mpa. This stress is insufficient to bring the structure to yield. At the free end of the structure the maximum displacement occurs (see Figure 5.9). By comparing the stress caused by the torque and the one caused by the thrust, it can be observerd that the stress of the torque is negligible.

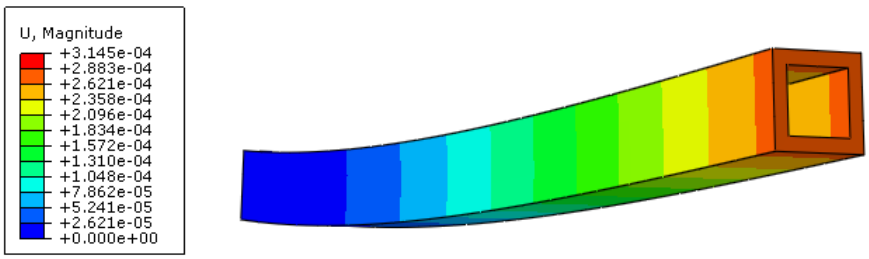

Figure 5.9: Deflection due to the maximu thrust of propeller.

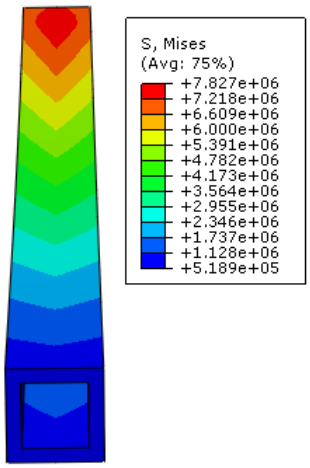

Figure 5.10: Deflection due to the maximum thrust of propeller.

5.3.3 Arm subjected to torque and thrust

In the real case thrust and torque act simultaenously so that the structure suffers stress at web and flange and deflects upwards and in the yaw plane. This is depicted in Figure 5.11 and Figure 5.12. The maximum stress is localized at the root of the arm with a value of 7.9 Mpa and a maximum displacement of $3.19x10^{-}4$ m is found at the tip.

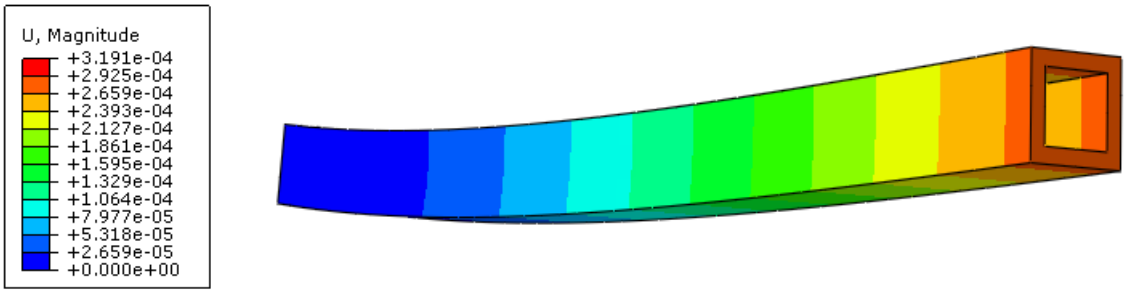

Figure 5.11: Deflection due to torque and maximum thrust of propeller.

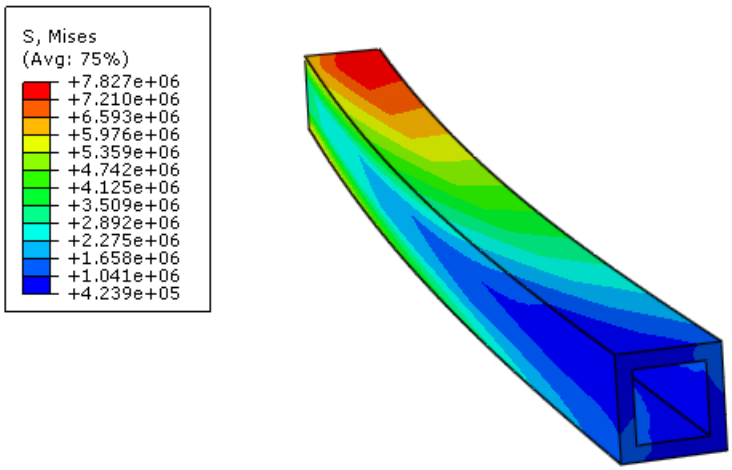

Figure 5.12: Stress due to torque and maximum thrust of propeller.

5.4 Carbon fiber tube

Another common material used to construct the frame is carbon fiber-reinforced thermoplastic. It is widely used in the aerospace industry due to its high stiffness and high strenght to weight ratio. The binding polymer is often a thermoset resin such as epoxy. Table 5.3 presents the mechanical properties of Carbon Epoxy.

Figure 5.13: Quadrotor frame made out of carbonfiber tubes.
Source:"*www.hobbyking.com/hobbyking/store/__22397__Turnigy_Talon_Carbon_Fiber_Quadcopter_Frame.html*"

Properties	**Carbon Epoxy**
Young Modulus 0° E_1 [GPA]	162
Young Modulus 90° E_2 [GPA]	7.93
In plane shear modulus G_{12} [GPA]	5.3
G_{13} (GPA]	5.3
G_{23} (GPA]	4
Poisson's ratio ν_{12}	0.35
Longitudinal tensile strength X_t [Mpa]	2899
Longitudinal compressive strengthX_c [Mpa]	1414
Transverse tensile strength Y_t [Mpa]	37
Transverse compressive strength Y_c [Mpa]	169
Longitudinal shear strength S_{12} (MPa) [Mpa]	169
Transverse shear strength S_{13} [Mpa]	169
Density ρ $[kg/m^3]$	1600

Table 5.2: Properties of composite materials.

Several manufacturers were investigated [6] [7] [8]. In order to save weight, the smallest carbon fiber tube was selected, modelled and analyzed on Abaqus to verify that it will withstand the loads and not suffer high deflections. The inner and outer diamater of the section are 6mm and 8mm respectively.

[6] *www.rockwestcomposites.com/*
[7] *www.acpsales.com/*
[8] *www.easycomposites.co.uk*

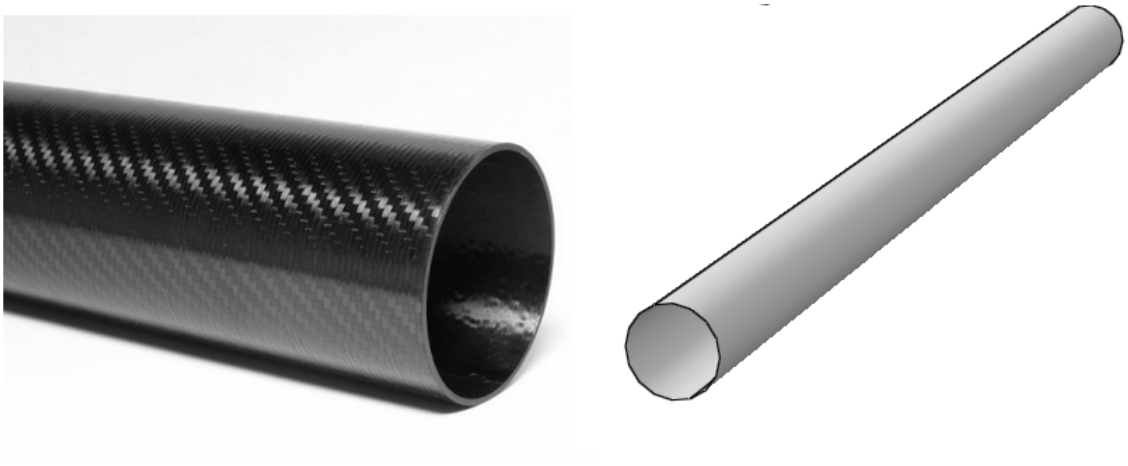

Figure 5.14: Left: Actual carbon fiber tube from manufacturer. Right: Abaqus model.

The same analysis performed on the aluminium bar is carried out on the carbon fiber tube. The results can be seen in figure 5.15 and figure 5.16, where both the effect of the thrust and the torque are included.

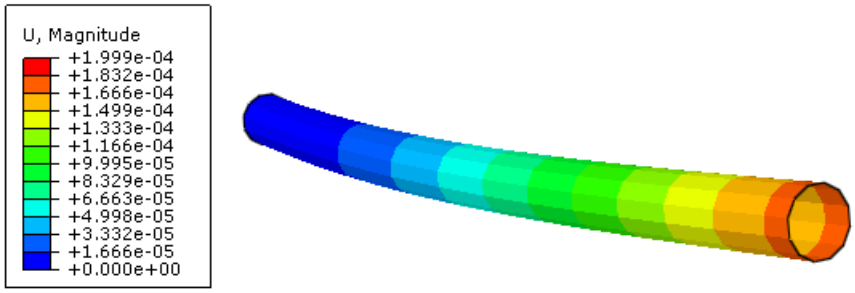

Figure 5.15: Deflection.

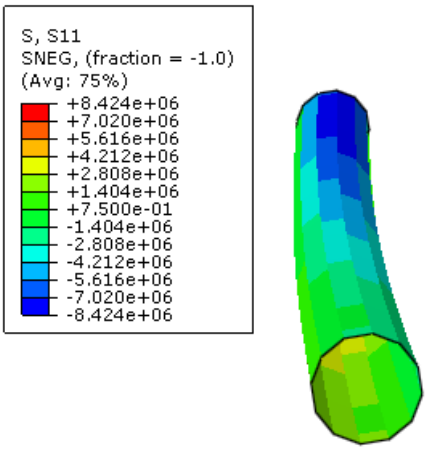

Figure 5.16: Longitudinal stress.

The maximum deflection can be found on the tip with a value of $2x10^{-}4$ m. For material failure the von Mises stresses can not be taken as a reference since the material is a composite. For unidirectional composite the most widely used failure criteria is maximum stress failure criterion (Tsai, 1987; Nahas,1986), which predicts that a material will fail when the magnitude of the stress in any direction exceeds its corresponding allowable level in that direction. The stresses found on the structure are in the longitudinal direction, with a maximum tensile stress of 8.4 Mpa on the bottom part and a maximum compressive stress of 8.4 Mpa on the upper part. These stresses are well under the limit of the material.

5.4.1 Comparison

	Maximum stress [MPa]	**Maximum deflection [m]**	**Mass [g]**
Aluminium bar	7.827	$3.191x10^{-}4$	47.5
Carbon fiber tube	8.4	$2x10 - 4$	24

Table 5.3: Properties of composite materials.

Carbon fiber tubes are selected to be the arm of the quadrotor. It offers a lower weight, a smaller deflection and the maximum stress encounteres is well below the limit of the material.

Chapter 6

Performance and dynamics

This chapter analyzes the 2D equations of motion [13] of the quadrotor considering momentum theory and blade element theory [14] [15]. Hover, climb and forward flight are studied. From the equations of motion important parameters such as position, velocity and power can be obtained. With the velocity and the respective power consumption and the analysis conducted in chapter 4 the endurance of the vehicle is obtained. Then the total area that the UAV is able to image is computed considering the values obtained in the camera analysis in chapter 3. The area that the quadrotor is able to inspect in one single flight is an important factor to know since it determines the viability of using UAVs for photovoltaic field inspections.

6.1 2D model of a quadrotor

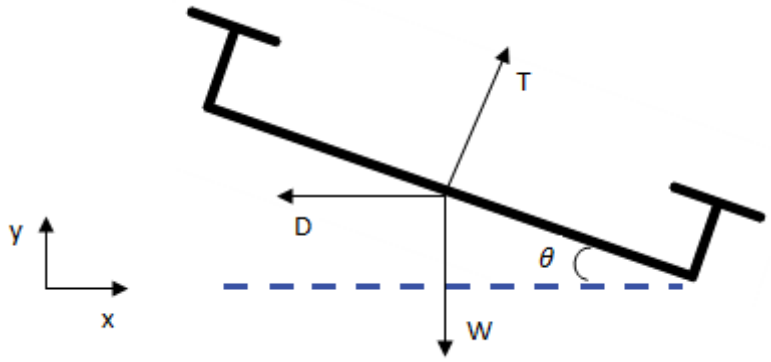

Figure 6.1: 2D model of a quadrotor.

The main forces acting on the center of gravity of a quadrotor are depicted in figure 6.1, where T is the thrust generated by the motors, W is the weight of the vehicle and D is the drag and is given by $\frac{1}{2}\rho S c_d \dot{V}^2$, where where S is the cross sectional area of the vehicle facing the flow, c_d is the drag coefficient, ρ is the air density and V is the freestream velocity. By taking summary of forces the linear equations of motions are given by:

$$m\ddot{x} = T\sin\alpha - D_x$$

$$m\ddot{y} = T\cos\alpha - W - D_y$$

.

Pitch is controlled by varying the motors speed. Producing a higher thrust with motor 2 than with motor 1 leads to a pitch torque increasing the pitch angle of attack. Nevertheless in the analysis conducted the rotational equation of motion for pitch will not be needed, in ascend and hover the pitch angle of attack remains zero (all motors spin at the same rate), and for forward flight it will be assumed that the vehicle is already inclined with an angle α, meaning that it is not necessary to produce a pitch torque to achieve a desired angle of attack.

6.2 Thrust according to blade element theory

To model the thrust generated by the propellers blade element theory is used. Blade element theory is the application of airfoil theory to the rotating blade. The equation of thrust is:

$$T = \frac{\rho A \sigma a \Omega^2 R^2}{2} \left(\frac{\theta_{0.75}}{3} - \frac{V_c + v_i}{2\Omega R} \right),$$

where ρ is the air density, A is the area swept by the rotor, σ is the solidity ratio and is expressed as the ratio of the blade area to the disc area $\sigma = \frac{Nc}{\pi R}$, where N is the number of blades, c is the chord of the blade and is a function of the radius R, a is the lift-slope factor and has a value of about 5.7, Ω is the angular velocity, $\theta_{0.75}$ is the pitch angle at three quarters radius, V_c is the inflow velocity prior entering the rotor and v_i is the induced velocity and is given by $v_i = -\frac{V}{2} + \sqrt{\frac{V}{4}^2 + v_h^2}$, where v_h is the induced velocity at hover and is given by $v_h = \sqrt{\frac{T}{2\rho A}}$. Combining the thrust according to blade element theory and the 2D equations of moment leads to:

$$m\ddot{x} = \frac{\rho A \sigma a \sin\alpha}{2} \left(\frac{\theta_{0.75}\Omega^2 R^2}{3} - \frac{\Omega R}{2} \left(\frac{\dot{x}\sin\alpha + \dot{y}\cos\alpha}{2} + \sqrt{\frac{(\dot{x}\sin\alpha + \dot{y}\cos\alpha)^2}{4} + v_h^2} \right) \right) - \frac{1}{2}\rho S c_d \dot{x}^2$$

$$m\ddot{y} = \frac{\rho A \sigma a \cos\alpha}{2} \left(\frac{\theta_{0.75}\Omega^2 R^2}{3} - \frac{\Omega R}{2} \left(\frac{\dot{x}\sin\alpha + \dot{y}\cos\alpha}{2} + \sqrt{\frac{(\dot{x}\sin\alpha + \dot{y}\cos\alpha)^2}{4} + v_h^2} \right) \right) - \frac{1}{2}\rho S c_d \dot{y}^2 - mg$$

The propeller geometry properties introduced for solving the system of 2 differential equations correspond to the APC 11x4.7 propeller described in section 4.3. The geometry parameters can be found in appendix A.2.

6.3 Hover and climb

For hover and climb the angle of attack α is zero, so that the velocity in the horizontal direction remains zero. Additionally for hover $\dot{y} = 0$. The differential equation to solve is then

$$m\ddot{y} = \frac{\rho A \sigma a \Omega^2 R^2}{2} \left(\frac{\theta_{0.75}}{3} - \frac{\frac{\dot{y}}{2} + \sqrt{\frac{\dot{y}}{4}^2 + v_h^2}}{2\Omega R} \right) - mg - -\frac{1}{2}\rho S c_d \dot{y}^2$$

Drag is given by $D = \frac{\rho S c_d \dot{y}^2}{2}$ where S is the cross sectional area of the vehicle facing the flow and c_d is the drag coefficient. When the quadrotor climbs the cross sectional area encountering the wind resembles to a flat plate.

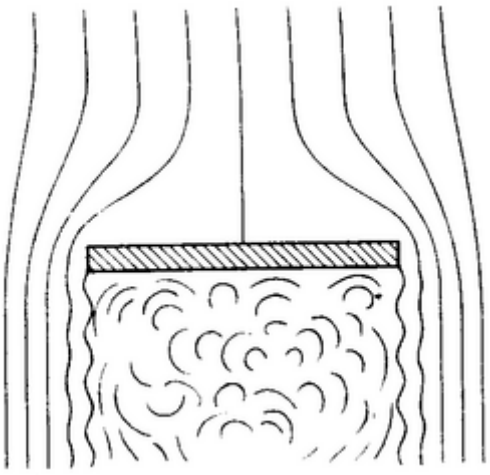

Figure 6.2: Streamlines of a flat plate normal to the flow.
Source:"$http://www.me.metu.edu.tr/courses/me410/exp6/exp6.html$"

The drag coefficient for a flat plate normal to the flow has a value in the vicinity of 1.2.

6.3.1 Results

Solving the differential equation for hover and climb leads to the following results:

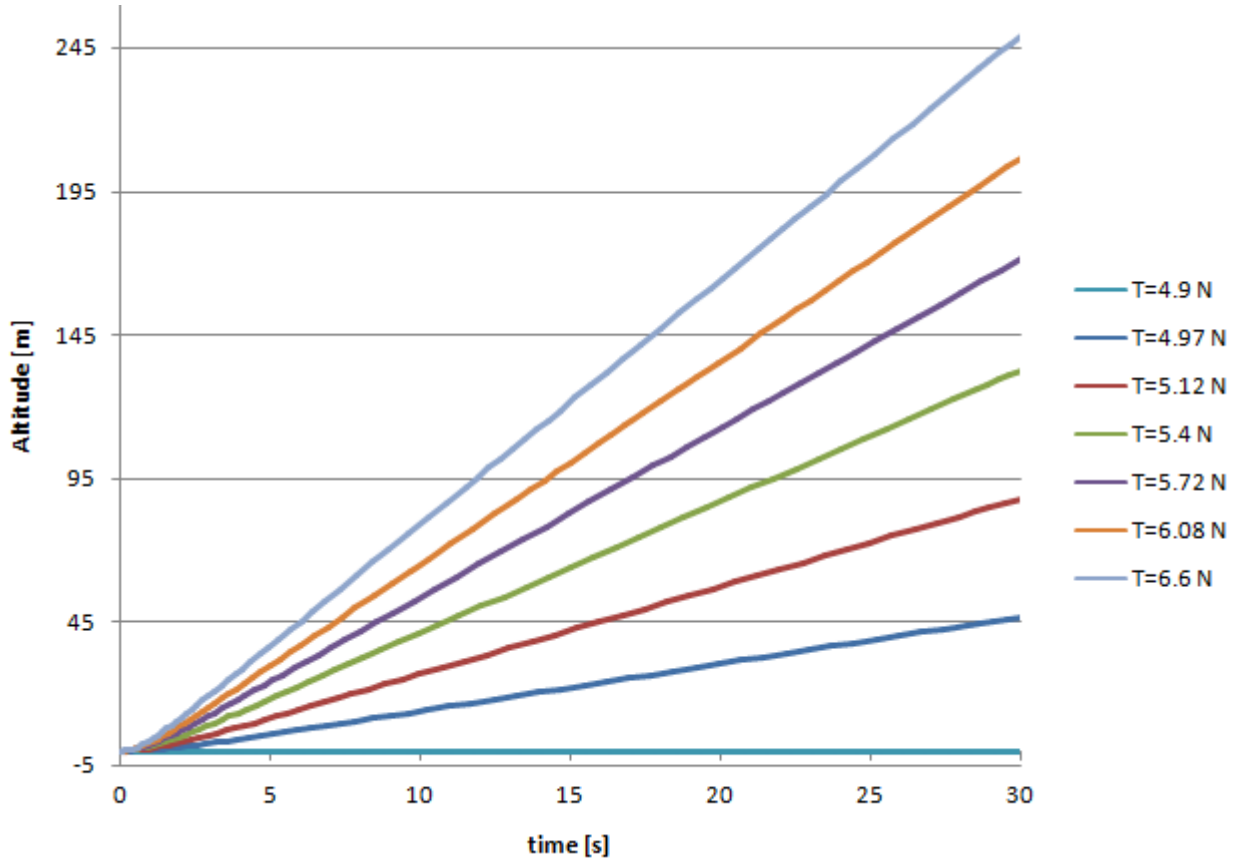

Figure 6.3: Climb and hover for different thrust settings.

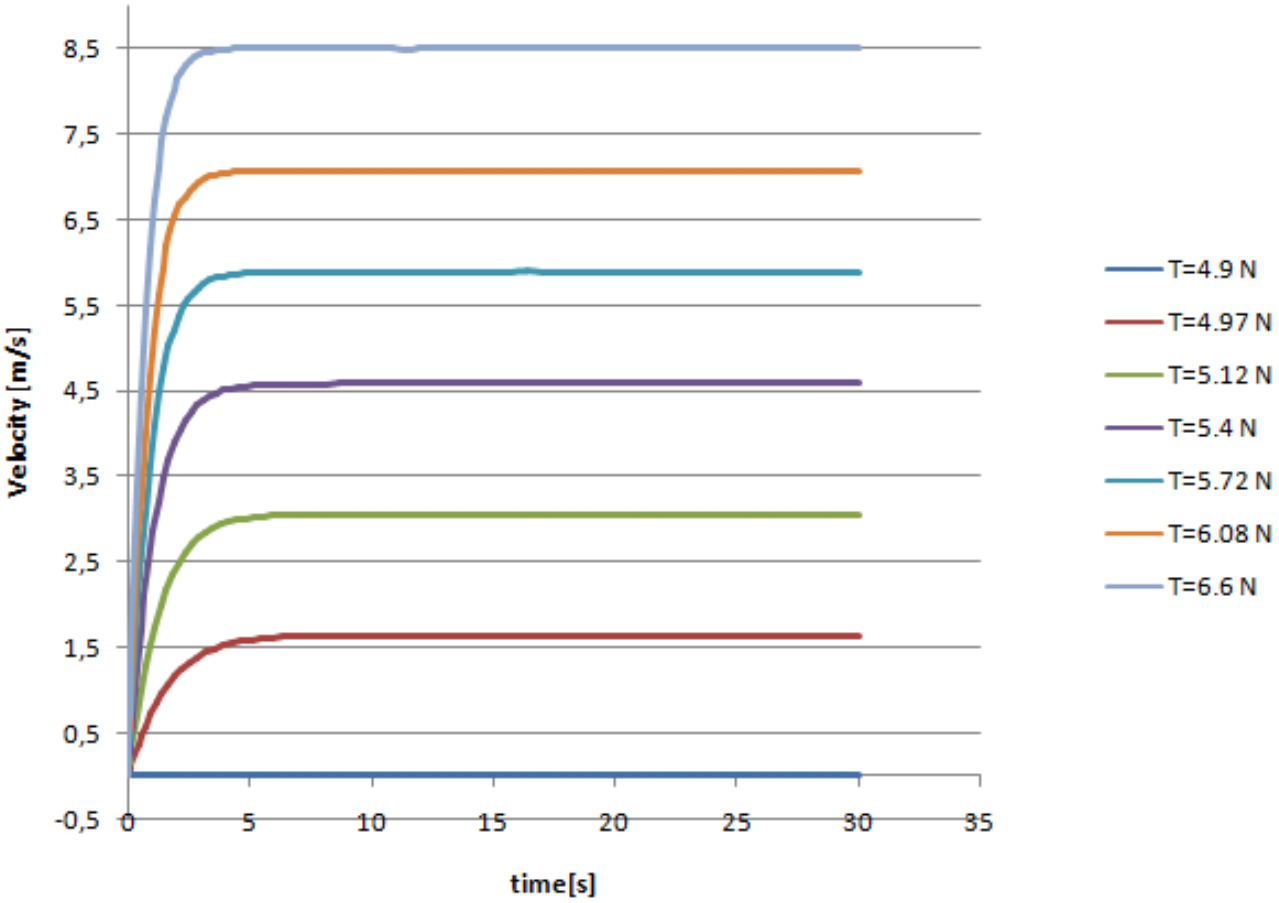

Figure 6.4: Velocity vs. time for different thrust settings.

With a thrust of 4.9 N the vehicle is hovering as can be observed in figure 6.3 and figure 6.4. Note that the value of thrust generated is per motor, since all motors are spinning at the same rate, each motor is lifting the same weight, i.e. one quarter of the total weight of the vehicle. It can also be seen that for higher thrust setting a higher velocity is achieved and therefore higher altitudes in the same periods of time are reached. In figure 6.4 it can be seen how the vehicle accelerates until the terminal velocity is reached.

The next step was computing the power required for each thrust setting by means of the following equation $P_i = T(\dot{y} + v_i)$. Note that the expression for power does only consider the induced power and not the profile power. The profile power is computed by considering that the profile power does not vary greatly with the level of thrust, provided the blade does not stall nor experience high compressibility drag rise. Then the profile power can be computed by $P_p = P_{tot} - P_i$. From the analysis conducted in chapter 4 the total power absorbed in hover is obtained. The value for the total power absorbed in hover is 69 Watts. P_i is computed with the previously presented equation and has a value of 40.11 W, so that the profile power turns to be 28.89 W.

T [N]	P total [W]	Current draw [A]	t to reach mission altitude [s]	Amp-hours
4.905	69	6.6	-	-
4.97	73.29	7.1	20.9	0.0412
5.12	77.24	7.5	11.8	0.0246
5.4	81.82	8	8	0.0178
5.72	86	8.4	6.2	0.0145
6.08	104.56	10.5	5.1	0.0149
6.6	117.8	12	4.9	0.0163

Table 6.1: Performance results for hover and climb.

Table 6.1 relates the thrust setting,the power consumption, the current draw and the time to reach the mission altitude with the ampere-hours of battery charge comsumed during climbing. The power for each thrust setting is computed as explained in the previous paragraph, the current draw is obtained by looking at figure 4.8, the time to reach mission altitude, which is 32 m, is seen in figure 6.3 and ampere-hours of charge consumed is computed by multiplying the current draw with the time to reach mission altitude. One can observe that flying at a lower thrust setting does not mean the power consumed will be lower than at a higher thrust setting. There is an optimum thrust setting where the consumption to reach mission altitude will be the lowest. The thrust setting corresponds to 7.72 N.

6.4 Forward flight

In forward level flight the system of two differential equations presented in section 6.2 are solved. The results can be seen in figure 6.5 and figure 6.6

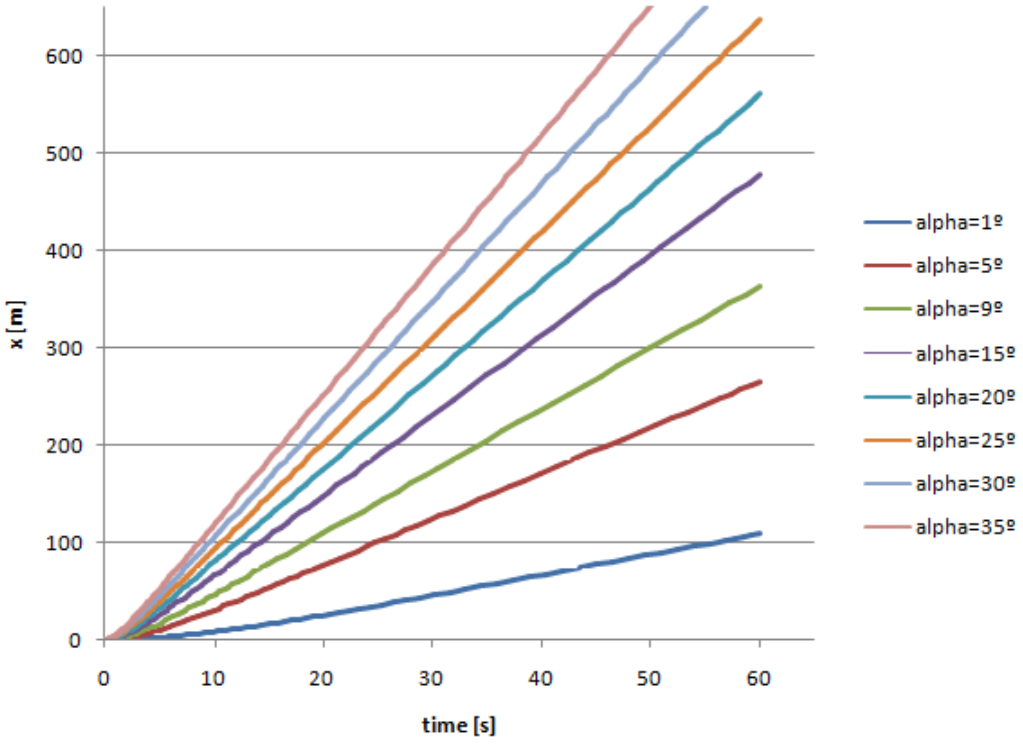

Figure 6.5: x vs. time in forward level flight for different angle settings

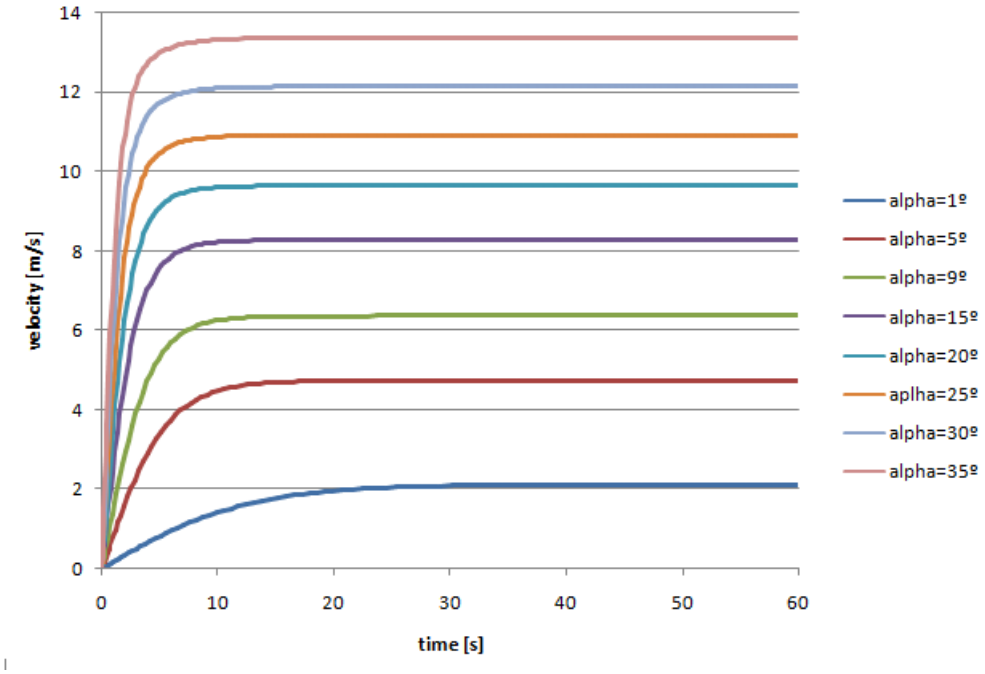

Figure 6.6: Velocity vs. time in forward level flight for different angle settings.

The higher the angle of attack, the higher the component of thrust in the horizontal axis is, and therefore higher velocities are achieved.

Angle of attack [degrees]	**T [N]**	**P total [W]**	**Current draw [A]**	**Endurance [km]***
1	4.905	69.12	6.65	3.4
5	4.924	70.2	6.8	7.4
9	4.966	71.92	6.9	9.9
15	5.1	76.32	7.5	11.9
20	5.22	80.89	7.85	13.2
25	5.4	87.29	8.6	13.6
30	5.66	95.18	9.5	13.8
35	6	105.6	10.5	13.7

Table 6.2: Performance results for forward level flight.

Table 6.2 summarizes the performance for forward level flight. To compute the endurance following equation is used: $Endurance = \frac{vc_{bat}}{nI}$, where v is the quadcopter terminal velocity, c_{bat} is the batteries capacity, I is the current draw by one single motor and n is the number of motors (4). One can see that the maximum endurance is achieved when the vehicle is flying at an angle of attack of 30 degres. It is possible that the vehicle might not be able to fly at the velocity corresponding to the angle of attack of 30 degrees since the blur caused by a moving camera has to be taken into account. By multiplying the endurance by the horizontal field of view, the area that the quadcopter is able to inspect is obtained. The area that is inspected on a single flight is 37.2 ha.

*Note that the values for endurance are overestimated. In the presented analysis the vehicle is flying only in forward flight, while in the real case turns will be required. It is assumed the vehicle is flying in a calm day with no wind. In the real case the microcontroller is sending

constant conrrections to the electronic speed controllers to mantain altitude and velocity, while in this analysis the four motors are operating all the time at the same rate. In this analysis the power consumed by the thermal camera and the microcontroller are not included, which would also reduce the endurance.

Chapter 7

Selection of missing components and cost analysis

In chapter 3 the thermal camara was selected; in chapter 4 the propulsion system consisting of the battery, electronic speed controller, motor and propeller was chosen. In this chapter the missing components of the quadcopter are listed and selected.

7.1 Flight controller

The flight controller is the computer of the quadcopter; it receives measurements from the sensors and sends corrections to the electronic speed controllers so that the vehicle flies in the desired direction. There are a few properties of the flight controller to consider when selecting a suitable one [16]:

Inertial measurement unit (IMU) included
The sensors responsible of measuring velocities, accelerations and orientation of the vehicle may be included in the controller or not.

Gyro Stabilization
The ability to easily keep the quadcopter stable and level under the control of the pilot. This is a standard feature of all flight controllers.

Self Leveling
When the pilot lets go of the pitch and roll stick on the transmitter, the quadcopter stays level.

Care Free
The pilot can control the copter as if it is pointing in its original direction as the orientation of the copter changes.

Altitude Hold
The ability to hover a certain distance from the ground without having to manually adjust the throttle.

Return Home
The quadcopter is able to return to the location where it took off.

Position Hold
The flight controller sends the order to hover at a specific location. Useful in case a photograph of a specific area wants to be taken.

Waypoint Navigation

The quadcopter is able to fly autonomously by following a set of previously defined waypoints. This is an important chracateristic since the vehicle is then capable of autonomously inspecting photovoltaic fields.

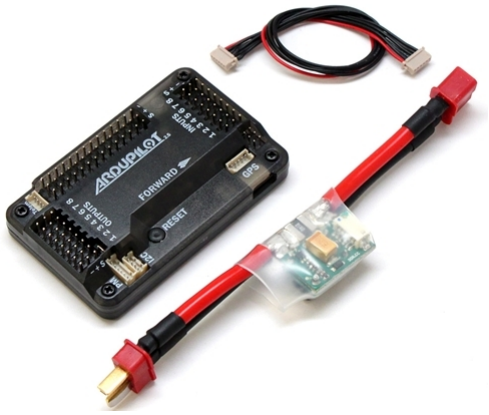

Figure 7.1: Arducopter APM 2.5
Source:
"$http://copter.ardupilot.com/wiki/common-apm25-and-26-overview/?lang=es$"

The Arducopter APM 2.5 is a complete open source autopilot system. It includes all of the above mentioned characteristics, including the waypoint navigation system which allows for autonomous flying, therefore it is chosen to be the flight controller of the quadcopter.

7.2 Transmitter and receiver

The transmitter is the electronic device which allows controlling the UAV. An important parameter of transmitters are the channels. Each channel allows controlling 1 degree of freedom of the UAV. In case of a quadcopter four channels is the minimum, so that pitch, roll, throttle and yaw can be controlled.

Figure 7.2: Turnigy 9x RC transmitter
Source:
"*www.hobbyking.com/hobbyking/store/__8992__Turnigy_9X_9Ch_Transmitter_w_Module_8ch_Receiver_Mode_2_v2_Firmware_.html*"

The turnigy 9x RC transmitter is selected to be the transmitter. It also includes the receiver.

7.3 Cost analysis

Component	**Name**	**Quantity**	**Cost [$]**
Thermal Camera	Flir Tau 2 640	1	9646
Motor	Turnigy AX-2810Q-750	4	83.4
Propeller	APC 11x4.7	4	4.8
Battery	Turnigy NanoTech 6000	2	97.14
Electronic Speed controller	Q Brain ESC	1	29.92
Flight controller	Arducopter APM 2.5	1	159.99
Transmitter and Receiver	Turnigy 9x	1	59.99
Total			10081

Table 7.1: Cost analysis

Chapter 8

Conclusions

A preliminary design of a vehicle capable of inspecting photovoltaic fields has been presented.

Photovoltaic energy is seeing years of extraordinary growth and it is expected that it will continue expanding. Nevertheless there are anomalies that affect the efficiency of these systems and therefore it is of paramount importance monitoring photovoltaic panels. Combining a thermal camera with a UAV provides a fast and accurate method to detect these anomalies.

From the wide variety of UAV configurations, a quadcopter was chosen to be the most suitable vehicle for this mission. Due to its ability for vertical take off and landing, slow flight and hover it offers a lower risk against craches and great advantages for aerial photography.

Once the airframe configuration of the UAV was selected, a payload analysis was performed. Several thermal cameras and their specifications were studied to see which would be the most appropriate. The weight and the field of view were the scoring paramenters when chosing the thermal camera.

The propulsion system consiting of propeller, motor, electronic speed controller and battery were then selected. To narrow down the vast combination of propulsion systems that exist, quadcopters whose mission the aerial photography is were analyzed and then motors, propellers and batteries with similar parameters were searched. The efficiency of several motors was then compared in order to select one and the propeller was chosen following the design rule that at 50% of maximum thrust the vehicle should be hovering. With help of a weight estimate and the requirement that the total weight of the vehicle must be bellow 2 kg the battery was selected.

A structural analysis was then conducted, to determine the material to be used for the frame and the section of the arms. Before performing the structural analysis on Abaqus, it was ensured that the chosen dimensions for the beams were the ones available from manufacturers. An aluminium hollow square beam and a carbonfiber tube were tested by applying a point load and a torque at the free end, simulating the forces that the propeller would produce. The carbonfiber tube were chosen to be the arms of the frame because they offered a lower weight and the stresses found were well bellow the materials limit.

To have an estimate of the endurance of the vehicle, the 2D equations of motions combined with blade element theory were studied. Performance paramenters for hover, climb and forward flight were obtained by solving the system of two differential equations. The optimum thrust setting to obtain maximum endurance was found out and the preliminary results shows a promising value for the area of inspection of the vehicle in a single flight.

At last the flight controller, transmitter and receiver were selected and the budget required to buy all the components was showed.

8.1 Future work

For a preliminary design a lot of parameters have been considered to demonstrate the viability of the project, nevertheless a more detailed design is pending.

A deeper analysis on the thermal camera has to be carried out. The shutter speed of the camera and the frames per second at wich the camera records a video have to be analyzed in order to avoid blur due to a too high vehicle's speed.

A cad model to determine how all the components are going to be positioned and assembled and derive more accurate dimensions for the structure.

A more detailed structural analysis including the centre plate and the skids has to be done.

Buy all the components and compare experimental values with theoretical values: find out if the computed mission altitude is accurate enough to detect most of the anomalies, test the motors to proof their efficiency, thrust generation and power consumption and a flight test to check the actual endurance of the vehicle.

Appendix A

Appendices

A.1 Thermal camera technical specifications

Specifications

SYSTEM OVERVIEW

System Type	Uncooled LWIR Thermal Imager
Tau 2 640	640 x 512 VOx Microbolometer
Tau 2 336	336 x 256 VOx Microbolometer
Tau 2 324	324 x 256 VOx Microbolometer
Pixel Size	17 µm (**Tau 2** 640, 336); 25 µm (**Tau 2** 324)
Spectral Band	7.5 - 13.5 µm
Performance	<50 mK @ f/1.0

OUTPUTS

Analog Video	Field-switchable between NTSC and PAL
Tau 2 640	30/60Hz (NTSC); 25Hz/60Hz (PAL); <9Hz option for export (factory set)
Tau 2 336, 324	30/60 Hz (NTSC); 25/50 Hz (PAL) ; <9Hz option for export (factory set)
Digital Video	8- or 14-bit serial LVDS; 8- or 14-bit parallel CMOS; 8-bit BT.656

OPERATION & CONTROL

Image Control	Invert, revert, continuous digital zoom, dynamic zoom & pan, digital zoom presets,polarity, false color or monochrome, isotherms, AGC, second generation digital detail enhancement (DDE), image optimization (BPR, NUC & AGC'd video),Active Contrast Enhancement (ACE, Information Based Histogram Equalization (IBHEQ), Smart Scene Optimization (SSO), settable splash screens
Camera Control	Manual via SDK & GUI, dynamic range switching (**Tau 2** 324 only)
Signal Interface	Camera Link (Expansion Bus Accessory Module), discrete I/O controls available, RS-232 compatible (57,600 & 921,600 baud), external sync input/output, power reduction switch (removes analog video)
FFC Duration	<0.5 sec

PHYSICAL ATTRIBUTES

Size	1.75" x 1.75" x 1.75" (less lens)
Mounting Interface	6 attach points in lens mount, M2 x 0.4 on 3 sides, 2 per side (sealable bulkhead mounting feature on lens barrel [M29 x 1.0], WFOV only)

POWER

Input Voltage	4.0 – 6.0 VDC
Primary Electrical Connector	50-pin Hirose
Power Dissipation	~ 1.0 W (**Tau 2** 324 & 336); <1.2 W (**Tau 2** 640); <1.3W (Tau 2 640/60Hz)
Time to Image	<5 seconds (**Tau 2** 640); <4 seconds (**Tau 2** 336 and 324)

ENVIRONMENTAL

Operating Temperature Range	-40° C to +80° C external temp
Storage Temperature Range	-55° C to +95° C external temp
Scene Temp Range	High gain: -40°C to +160°; Low gain: -40°C to +550°
Shock	200 g shock pulse with 11 msec sawtooth
Temperature Shock	5°/min
Vibration	4.3 g 3 axes, 8 hours each
Humidity	5 - 95% non-condensing
Operational Altitude	+40,000 feet
ROHS, REACH, and WEEE	Compliant

Tau 2

Lens Data



		7.5 mm	9 mm	13 mm
		TAU 2 WIDE FIELD OF VIEW (WFOV) MODELS[1]		
		f/1.25 (**Tau 2** 640 = f/1.4)	f/1.25 (**Tau 2** 640 = f/1.4)	f/1.25
FOV[3] (h x v)	**Tau 2** 640 (17µ 640 x 512)	90° x 69°	69° x 56°	45° x 37°
	Tau 2 336 (17µ 336 x 256)	45° x 35°	35° x 27°	25° x 19°
	Tau 2 324 (25µ 324 x 256)	63° x 50°	49° x 39°	35° x 28°
iFOV (mrads)	**Tau 2** 640 (17µ 640 x 512)	2.267	1.889	1.308
	Tau 2 336 (17µ 336 x 256)	2.267	1.889	1.308
	Tau 2 324 (25µ 324 x 256)	3.333	2.778	1.923
Minimum Focus Distance[4]	All	2.5 cm	3 cm	8 cm
Length[5]	All	19 mm	19 mm	19 mm
Diameter		29 mm	29 mm	29 mm
Weight (Camera + Lens)		<71 g	72 g	<70 g
Detection, Recognition, Identification (DRI)[6] **Typical/Best Conditions** (range in meters)	**Tau 2** 640 & 336 - Man	D = 210/235 R = 52/60 I = 26/30	D = 250/285 R = 63/71 I = 31 /36	D = 390/440 R = 95/112 I = 47/56
	Tau 2 640 & 336 - Vehicle	D = 580/730 R = 150/180 I = 58/92	D = 720/880 R = 175/220 I = 88/108	D = 1,080/1340 R = 275/340 I = 140/170
	Tau 2 324 - Man	D = 170/185 R = 42/43 I = 21/23	D = 205/230 R = 52/57 I = 26/28	D = 300/330 R = 74/82 I = 37/41
	Tau 2 324 - Vehicle	D = 480/570 R = 120/140 I = 60/72	D = 590/700 R = 150/175 I = 74/88	D = 840/1000 R = 215/250 I = 108/125

1 – All WFOV lenses are integrated directly into a common lens holder with an internal O-ring that furnishes an IP-67 rating at the front surface. All WFOV lenses are M24 x 0.5 inside thread. Outside thread is M29 x 0.5.

2 – NFOV lenses are M34 x 0.3 inside thread.

3 – Digital output used for FOV calculation.

4 – Minimum focus distance for WFOV cameras is measured with the lens unscrewed to the point just before the O-ring groove becomes visible; for NFOV cameras it is measured one complete revolution after the lens first engages the lens flange.

5 – Length is measured from the front, flat surface of the lens holder to the end of the lens.

6 – DRI values shown are nominal values and should be used as estimates only. Exact DRI calculations depend on a wide variety of conditions. For more information, please contact FLIR.






19 mm	25 mm	35 mm	50 mm	60 mm	100 mm
		TAU 2 NARROW FIELD OF VIEW (NFOV) MODELS[2]			
f/1.25	f/1.1	f/1.2	f/1.2	f/1.25	f/1.6
32° × 26° 17° × 13° 24° × 19°	25° × 20° 13° × 10° 18° × 15°	18° × 14° 9.3° × 7.1° 13° × 10°	12.4° × 9.9° 6.5° × 5.0° 9.3° × 7.3°	10.4° × 8.3° 5.5° × 4.2° 7.7° × 6.1°	6.2° × 5.0° 3.3° × 2.5° 4.6° × 3.7°
0.895 0.895 1.316	0.680 0.680 1.000	0.486 0.486 0.714	0.340 0.340 0.500	0.283 0.283 0.417	0.170 0.170 0.250
16 cm	30 cm	60 cm	1.5 m	2.3 m	7 m
19 mm 29 mm <70 g	30 mm 42 mm 112 g	39 mm 42 mm 150 g	62 mm 58 mm 280 g	62 mm 61 mm 200 g	110 mm 82 mm 479 g
D = 570/640 R = 144/160 I = 72/80	D = 820/930 R = 210/230 I = 104/116	D = 1140/1280 R = 280/320 I = 142/160	D = 1500/1700 R = 380/430 I = 190/215	D = 1750/2000 R = 450/510 I = 225/255	D = 2450/2950 R = 650/750 I = 330/380
D = 1,550/1950 R = 400/500 I = 200/250	D = 2200/2800 R = 580/710 I = 290/360	D = 3000/3850 R = 800/950 I = 200/295	D = 3900/5100 R = 1060/1320 I = 540/660	D = 4500/6000 R = 1240/1560 I = 640/780	D = 6000/8800 R = 1750/2300 I = 900/1160
D = 450/490 R = 112/124 I = 56/62	D = 590/650 R = 148/165 I = 75/85	D = 800/880 R = 200/225 I = 105/112	D = 1125/1280 R = 290/320 I = 145/160	D = 1320/1500 R = 340/380 I = 170/190	D = 2075/2400 R = 540/600 I = 270/300
D = 1,280/1500 R = 330/375 I = 165/190	D = 1650/1950 R = 430/500 I = 215/250	D = 2250/2700 R = 590/680 I = 290/340	D = 3100/3800 R = 810/970 I = 415/490	D = 3600/4600 R = 960/1160 I = 480/580	D = 5300/7100 R = 1500/1840 I = 760/920

Tau 2 Part Number Configuration Guide (Ex: 46640019H-FPNLX)

46	640	019	H	-	F	P	NL	X
SHUTTER TYPE	RESOLUTION	LENS FOCAL LENGTH	LENS COATING		VIDEO SPEED	TAU TYPE	OEM INFO LOGO	EXPANSION CARD
46 = Standard 47 = Shutterless 66 = Standard *(640/60Hz only)* 67 = Shutterless *(640/60Hz only)*	640 (640 × 512) 336 (336 × 256) 324 (324 × 256)	001 = no lens 007 = 7.5 mm 009 = 9 mm 013 = 13 mm 019 = 19 mm 025 = 25 mm 035 = 35 mm 050 = 50 mm 060 = 60 mm 100 = 100 mm	H = Hard Carbon A = High Durability X = No Lens		F = Fast (60 Hz, 50 Hz) S = Slow (7.5 Hz, 8.3 Hz)	P = Performance	NL = No Logo *Also used for OEM ID*	X = No Card

A.2 Propeller geometry

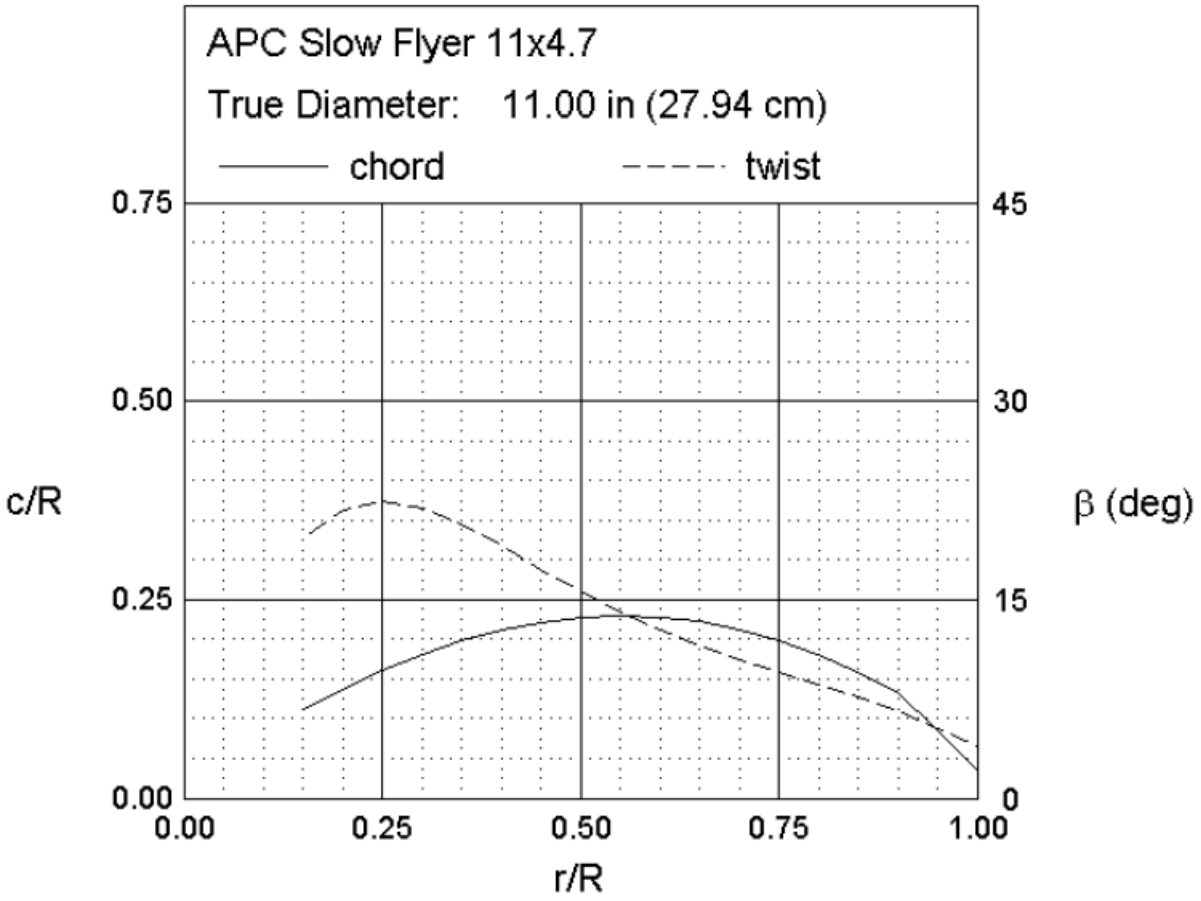

Figure A.1: Propeller geometry

Bibliography

[1] Masson, Gaëtan; Orlandi, Sinead; Rekinger, Manoël *Global market outlook for photovoltaics 2014-2018* 2014: European Photovoltaic Industry Association (EPIA), Brussels

[2] Buerhop, Claudia; Ulrike, Jahn; Hoyer, Ulrich; Lerche, Bernd; Wittmann, Stephan *Überprüfung der Qualität von Photovoltaik- Modulen mittels Infrarot-Aufnahmen* 2007: Abt. 3: Thermosensorik und Photovoltaik, Erlangen.

[3] Austin, Reg *Unmanned aircraft systems, UAVS design, development and deployment* 2010: John Wiley & Sons Ltd, West Sussex.

[4] Balas, C *Modelling and linear control of a quadrotor* 2006-2007 Cranfield University

[5] $http://blog.oscarliang.net/build-a-quadcopter-beginners-tutorial-1/$

[6] $http://www.academiatesto.com.ar/cms/?q=ifov$

[7] Avidan, Shai *Image Processing Applications a.k.a Computational Photography* Faculty of Engineering Tel-Aviv University

[8] Donohue, John *Introductory review of target discrimination criteria* 1991: Dynamics research corporation, Wilmington.

[9] http://www.trec.com/johnsoncriteria.htm

[10] Miller, Lucien *How to use the Multirotor Motor Performance Data Charts* Innovative Designs, Inc.

[11] Bourke, Jim *Understanding electric power systems* 1998

[12] von Mises, R. (1913). Mechanik der festen Körper im plastisch deformablen Zustand. Göttin. Nachr. Math. Phys., vol. 1, pp. 582–592.

[13] García Carrillo, L.R; Dzul López, A.E; Lozano, R.; Pégard, C. *Quad rotorcraft control vision-based hovering and navigation* 2013: Springer

[14] Seddon J. *Basic helicopter aerodynamics* 1990:BSP professional books

[15] Wayne, Johnson *Helicopter Theory* 1980:Dover publications, INC. New York

[16] $http://robot-kingdom.com/best-flight-controller-for-quadcopter-and-multicopter/$